STUDY OF ELECTRODE PATTERNS FOR THE DEVELOPMENT OF PIEZOELECTRIC STAGES

M.Tech. Thesis

By

Rahul Raj Khare

DISCIPLINE OF METALLURGY ENGINEERING AND MATERIAL SCIENCE

INDIAN INSTITUTE OF TECHNOLOGY INDORE

JUNE 2017

STUDY OF ELECTRODE PATTERNS FOR THE DEVELOPMENT OF PIEZOELECTRIC STAGES

A THESIS

Submitted in partial fulfilment of the requirements for the award of the degree

of

Master of Technology

by

Rahul Raj Khare

DISCIPLINE OF METALLURGY ENGINEERING AND MATERIAL SCIENCE

INDIAN INSTITUTE OF TECHNOLOGY INDORE

JUNE 2017

INDIAN INSTITUTE OF TECHNOLOGY INDORE

CANDIDATE'S DECLARATION

I hereby certify that the work which is being presented in the thesis entitled **Study of Electrode Patterns for The Development of Piezoelectric Stages** in the partial fulfilment of the requirements for the award of the degree of **Master of Technology** and submitted in the **Discipline of Metallurgy Engineering and Material Science, Indian Institute of Technology Indore**, is an authentic record of my own work carried out during the time period from May 2016 to June 2017 under the supervision of Dr. I.A.Palni, Associate Professor, IIT Indore, Dr. M.Anbarasu, Associate Professor, IIT Indore and Dr. Rahul Shukla, Scientific Oficer/E, RRCAT Indore.

The matter presented in this thesis has not been submitted by me for the award of any other degree of this or any other institute.

Rahul Raj Khare

This is to certify that the above statement made by the candidate is correct to the best of our knowledge.

Dr. I.A.Palani **Dr. M.Anbarasu**

Rahul Raj Khare has successfully given his M.Tech. Oral Examination held on **29th June 2017**.

Signature(s) of Supervisor(s) of M.Tech. Thesis
Date:

Convener, DPGC
Date:

Signature of PSPC Member #1
Date:

Signature of PSPC Member #2
Date:

ACKNOWLEDGEMENTS

This page is dedicated to acknowledge those responsible for playing a crucial role in the execution of this work. Without their guidance and help, the experience while constructing the dissertation would not have been so easy and well-organized.

With due respect and deepest regards, I would like to express my heart-felt gratitude and pleasure to **Dr. Rahul Shukla** for his encouragement, guidance and motivation throughout this project work. His important comments and suggestions have contributed a lot to my work and improved my understanding to the subject.

It gives me immense pleasure to express my gratitude to respected **Dr.Tapas Ganguly** (Head, Synchrotron Utilization Section, RRCAT) for providing me great opportunity to do dissertation in the prestigious research group of RRCAT. I would like to extend my special and sincere gratitude towards **Dr. Arvind Shrivastava**, and **Mrs. Pragya Tiwari** for their contribution in making this project materialize. I would like to thank **Mr. Bramhanand Sisodia**, **Mr. Ashok Kumar**, **Mr. M.P. Kamadh**, **Mr. Pawan Kumar** and all other crew for their sincere help during the project work.

I also thank **Dr Manoj Kumar Gupta** and members of Project placement committee for selecting me for project work at RRCAT. I also express my sincere gratitude to **Mr. Nikhil Pujari**, **Mr. Gowtham Beera**, **Mr. Jinoop A.N.**, **Mr. Shubham Saxena** and all the members, who helped me directly or indirectly throughout the project work.

I express my special thanks to **Dr. I.A.Palni** (Associate Professor, Department of Metallurgy Engineering and Material Science, I.I.T. Indore) and **Dr. M.Anbarasu** (Associate Professor, Department of Electrical engineering, I.I.T. Indore) for his guidance and encouragement. Lastly, but not the least I would like to thank all my friends of RRCAT, Indore and colleagues of I.I.T. Indore who helped me directly or indirectly throughout the course of this work.

The words in my acknowledgment seem to be inadequate to express my dense gratitude to my parents and family for their love, care, inspiration and all the supports to complete my work. At last I extend my warm regards to all people who directly or indirectly helped me.

Last but not the least I would like to thank the almighty God.

Rahul Raj Khare

DEDICATED TO
MY BELOVED
PARENTS

सत्यमेव जयते

GOVERNMENT OF INDIA
DEPARTMENT OF ATOMIC ENERGY

RAJA RAMANNA CENTRE FOR ADVANCED TECHNOLOGY
INDORE- 452013, INDIA

CERTIFICATE

This is to certify that Mr. Rahul Raj Khare, a student of Master of Technology in Discipline of Metallurgy Engineering and Material Science, Indian Institute of Technology Indore, has completed the project work entitled **"Study of Electrode Patterns for The Development of Piezoelectric Stages"** at Synchrotrons Utilization Section (SUS), RRCAT, Indore during the period from May 2016 to June 2017.

We wish him all professional success in his future.

Dr. Tapas Ganguli
Section Head,
Synchrotron Utilisation Section
Raja Rammana Centre for Advanced
Technology, Indore

Dr. Rahul Shukla
Scientific Officer/E,
Synchrotron Utilisation Section
Assistant Professor,
Homi Bhabha National Institute
Raja Rammana Centre for Advanced
Technology, Indore

ABSTRACT

Piezoelectric stages have some promising application in the field of laser beam scanning and steering, micro projection displays and various micro positioning systems. Generally, the actuation mechanism of such Piezo stages is consisting of Unimorph/Bimorph actuators. In this research work, a novel Monolithic Piezoelectric Stage (MPS) is conceptualized and simulated. The MPS, with the help of Interdigitated Electrode pattern (IDE), is able to perform actuation like Tilting along X and Y axis and Translation in Z direction without the use of any subsequent or passive layer. Tilting of 0.55^o and Translation of 28 μm using a potential of 40 volts is simulated for the device having foot print of 20 mm^2. Comparison of actuation using Parallel Plate Electrode (PPE) and IDE is also discussed and parametric study and optimisation of IDE geometry has been done to enhance the performance of the device.

Abrasive Water Jet Machining (AWJM) has been tried to fabricate the device and the challenges faced during the fabrication procedure and reasons for the failure in fabrication of device is discussed in this work. Alternative method for fabrication using diamond saw cutting and grinding which results in decrement of piezoelectric coefficient of the material is also discussed in this research work.

Table of Contents

List of Figures

List of Tables

Chapter 1

Introduction

Micro-Electro-Mechanical Systems (MEMS) technology is based in microelectronics fabrication methods. The wide variety of materials available in this technology delivers advantages such as miniaturization and multiple components on a single chip for integrated Microsystems. MEMS are the systems with electrical and mechanical parts where at least one dimension are kept in micrometre. In MEMS, there are many types of micro-stages which are classified according to their actuation principle such as electrostatic micro-stage, thermal micro-stage, piezoelectric micro-stage and electromagnetic micro-stage [1].

Multi-axis actuation devices are required in a wide variety of applications, including manipulation of microgrippers [2], vibration damping for image stabilization [3], disk-drive protection [4], and probe-based microscopy and data-storage [5], optical endoscopy [6] and calibration of inertial sensors like gyroscope and accelerometer [7], [8]. Various methods are used for actuation of miniaturized stages like piezoelectric, electrostatic, and electromagnetic to produce displacement in the range of few tens to hundreds of micrometre. The advantage of piezoelectric stage lies in the precision, low power consumption and higher reliability associated with it. Also, piezo stage forms a monolithic structure useful for many applications.

The utilization of microfabrication techniques like Electro Discharge Machining (EDM), Abrasive Jet Machining (AJM), Laser Beam Machining (LBM), Electron Beam Machining (EBM), Electro-chemical Machining (ECM) are limited of faster manufacturing rate, lesser accuracy and repeatability, low aspect ratio and tapering on the side walls of structures. Bulk processed piezoceramic Lead Zirconate Titanate (PZT; Pb(Zr1-*x*Ti*x*)O3) offers significant potential for the development of high-performance microscale piezoelectric transducers. Various fabrication techniques like reactive ion etching (RIE) [9], direct machining or milling using diamond tools [10], Ultrasonic micromachining [11], laser ablation [12] and Micro powder blasting [13] etc.

1.1 Motivation

E.E. Aktakka et. al. [14], have developed multi vibratory microstage for 3-DOF with the help of piezoelectric cantilevers. That microstage produces tilting motion along X and Y axis of 1.04° along each and translational motion along Z-axis of 19.6 μm, when the operating at voltage of 25 V. Microstage is fabricated by using DRIE method and silicon as wafer. Prakruthi Hareesh et. al. [15], presented a new method for achieving transverse bending mode actuation of piezoelectric devices microfabricated from homogeneous layers of bulk lead zirconate titanate (PZT) using Interdigitated electrode (IDE). This technique employs IDE on single side of substrate and takes the advantage of geometrical parameter of the electrode to engineer an optimized electric field gradient in the substrate. Nachiappan Chidambaram et. al. [16], demonstrated in their work that IDEs have the potential to harvest more energy than parallel plate electrode (PPE) structures because the former exploit the longitudinal piezoelectric effect, which is about twice as high as the transverse piezoelectric effect used by PPE structures.

In this dissertation work, a monolithic piezoelectric stage is designed, and analysed. The monolithic stage is made of bulk homogeneous PZT-5H piezoelectric plate. Piezoelectric stage is actuated by using a unique distributed electrode pattern. The challenges faced during the fabrication and the reasons for failure in fabrication is also mentioned.

This micro-stage will be helpful for various applications as follow:

i) In precision machining process like UV lithography, laser cutting microstage will be act as worktable or platform on which work piece is fixed which can be move very precisely with multi-DOF so that we can get much more flexibility during machining and; also time reduction in doing alignments.

ii) This microstage also used for calibrating MEMS gyroscope and accelerometer sensors. For validating performance of these devices, we need multi-vibratory stage. By using stage, we are able to examine how accurately these devices are working.

iii) These devices providing out of plane motion can be used as micro-mirrors for various functions like beam scanning and steering, projection displays, microscopy, z-stacking and focusing etc.

By observing such important applications of microstage in real life scenario, we motivate to design and develop a stage capable of performing out of plane motion, so appropriate piezoelectric based stage is to be design, develop, analyse and fabricate is the agenda of this work.

1.2 Research Objectives

1.2.1 Overall objective

The overall objective of this thesis is to develop a novel Monolithic Piezoelectric Stage able to perform tilting and translation motion with the use of a unique distribution of electrode pattern.

1.2.2 Intermediate Objectives

i) To develop a device from a homogeneous bulk plate of PZT-5H

ii) To gain actuation using a unique electrode pattern i.e. IDE in transverse mode.

iii) To get symmetric and uniform translation and tilting along the node points of the stage.

iv) To optimize the parameter of IDE to get desired actuation at minimum input.

1.3 Organisation of thesis

This thesis is divided into six different chapters. The thesis is organized as follows:

Firstly, Chapter 1 gives the introductory information about the MEMS and microstage. It also explains the motivation and objective of the dissertation work. The actuation mechanisms in MEMS, basic terminology of piezoelectricity and IDE, current scenario are described in chapter 2.

In Chapter 3, the dimensions of piezoelectric stage, IDE size and parameters is determined for uniform tilting and translation. Finite element simulation is done in COMSOL Multiphysics.

In Chapter 4, challenges faced during the fabrication process, selection of fabrication procedure results and discussion of simulation and fabrication techniques are discussed.

Work is concluded in last chapter and suggestions to improve performance of the piezoelectric stage are mentioned under future work in Chapter 5.

Chapter 2

Literature Review

This chapter gives the detailed information about the study and research work carried out in the past for the fabrication of various piezoelectric stages. The research work is majorly divided into categories having actuation methods and structure, available piezoelectric stages, and use of electrode for different actuation mode. The electrode patterns are used to set up an electric field gradient in the piezoelectric material to exploit the reverse piezoelectric effect. However, the piezoelectric materials are anisotropic and have different properties in different lattice planes. The properties can be altered using different electrode patterns and geometry.

The block diagram below shows the category in which this literature review is divided:

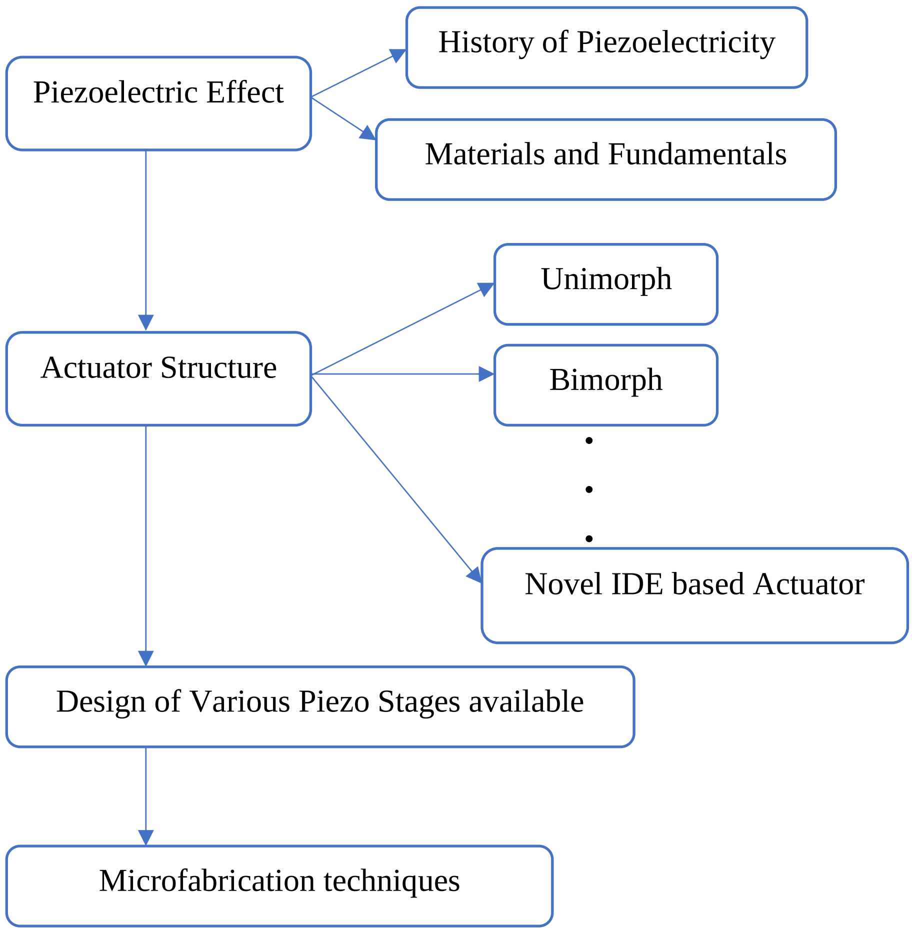

Figure 2.1 Block diagram of different media available for Piezoelectric stage.

2.1 Piezoelectric effect

If a stress is applied to certain crystals they develop an electric moment whose magnitude is proportional to the applied stress, this known as “Direct Piezoelectric Effect”.

That’s means a piezoelectric crystal produces an electric charge when we applied mechanical stress on it i.e. the substance is squeezed or stretched. Conversely, a mechanical deformation i.e. the substance shrinks or expands is produced when an electric field is applied that is known as “Indirect Piezoelectric Effect”. This effect is formed in crystals that have no centre of symmetry [17].

In order to create the piezoelectric effect, the polycrystal is heated under the application of a strong electric field. Each molecule of crystal has a polarization; one end is more negatively charged whether another end positively charged called as dipole. Because of heat, the molecules are moving more freely and the electric field forces all of the dipoles in the crystal to line up and face in the same direction.

2.1.1 The History of the Piezoelectric Effect

The direct piezoelectric effect was first seen in 1880, and was initiated by the brothers Pierre and Jacques Curie. Pyro-electricity is the ability of certain materials to generate a temporary voltage when they are under thermal loading i.e. heated or cooled. The change in temperature adjust the positions of the atoms slightly within the crystal structure, such that the polarization of the material changes. By using knowledge of pyro-electricity with understanding of crystal structures and behaviour, the Curie brothers demonstrated the first piezoelectric effect by using crystals of tourmaline, quartz, topaz, cane sugar, and Rochelle salt. From this demonstration, they have come to conclusion that quartz and Rochelle salt exhibited the most piezoelectricity ability at the time. The Curies, however, did not anticipate the converse piezoelectric effect, however Gabriel Lippmann withdraw converse effect mathematically from fundamental thermodynamic in 1881. Then Curies immediately authenticated the existence of the converse effect, gave quantitative proof of the complete reversibility of electro-elasto-mechanical deformations in piezoelectric crystals.

During World War I, first practical application for piezoelectric devices, which was the SONAR device introduced. This first use of piezoelectricity in SONAR made aware world of piezoelectricity and its various applications.

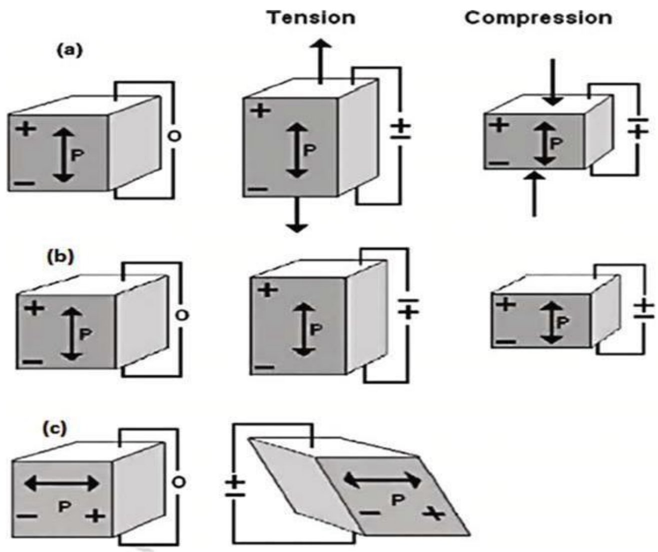

Figure 2.2. Schematic representation of the longitudinal direct (a) piezoelectric effects (b) converse piezoelectric effect (c) shear. [17]

During World War II, scientist in the US, Russia and Japan found materials, called ferroelectrics, which have piezoelectric constants many times greater than natural piezoelectric materials. Also after the quartz crystals were the first commercially used piezoelectric material in sonar detection applications, besides that scientists are curious for higher performance materials. This extraordinary research resulted in the evolution of barium titanate and lead zirconate titanate (PZT), two materials that had very specific properties suitable for particular applications [18].

2.2 Piezoelectric Materials

Table 2.1 Materials with piezoelectric property.

Crystals(natural)	Ceramics(man-made)
Quartz	Barium titanate (BaTiO3)
Rochelle salt	Lead titanate (PbTi3)

Topaz	Lithium niobate (LiNb3)
Sucrose (table salt)	Lithium tanalate (LiTaO3)

2.2.1 Fundamentals of the Piezoelectric Effect in Single Crystals and Ceramics

The piezoelectric ceramic is an anisotropic, so that physical constant relates both the direction of the applied mechanical or electric force and the directions perpendicular to the applied force. Piezoelectric coupling is described by a direct proportionality (linear relationship) between the first-rank tensor/vector (D or E) and the second-rank tensor (σ or S), the corresponding coupling coefficients dk_{ij} (also called charge piezoelectric coefficients) form a third-rank tensor. Hence, the piezoelectric governing equations may be written in the following form (i, j, k = 1, 2, 3):[17]

$$S_{ij} = dk_{ij}E_k$$

$$D_k = dk_{ij}\sigma_{ij}$$

The piezoelectric unimorph cantilever works in transverse mode and it is governed by the following equations [19]:

$$D = dE + \xi^T E \quad \text{(1)}$$

$$\varepsilon = s^E\sigma + dE \quad \text{(2)}$$

Where, σ . . . stress vector (*N/m*2) *ε* . . . strain vector (*m/m*)

E = vector of applied electric field (*V/m*)

ξ = permittivity (*F/m*)

d = matrix of piezoelectric strain constants (*m/V*)

S = matrix of compliance coefficients (*m*2/*N*).

D = vector of electric displacement (*C/m*2)

g = matrix of piezoelectric constants (*m*2/*C*)

β = permittivity component (*m/F*)

The superscripts denote a quantity which is held constant.

2.2.2 Piezoelectric constants

Piezoelectric Charge Constant, d: The piezoelectric charge constant, d, is the polarization generated per unit of mechanical stress (T) applied to a piezoelectric material or, it is the strain (S) generated in piezoelectric material per unit of electric field applied. The first subscript to d indicates the direction of polarization generated in the material when the electric field, E is zero. And second subscript is the direction of the applied stress or the induced strain, respectively.

d_{33}: Induced polarization in direction 3 (parallel to direction in which ceramic element is polarized) per unit stress applied in direction 3 or induced strain in direction 3 per unit electric field applied in direction 3.

d_{31}: Induced polarization in direction 3 (parallel to direction in which ceramic element is polarized) per unit stress applied in direction 1 (perpendicular to direction in which ceramic element is polarized) or induced strain in direction 1 per unit electric field applied in direction 3.

d_{15}: Induced polarization in direction 1 (perpendicular to direction in which ceramic element is polarized) per unit shear stress applied about direction 2 (direction 2 perpendicular to direction in which ceramic element is polarized) or induced shear strain about direction 2 per unit electric field applied in direction 1.

Piezoelectric Voltage Constant, g: The piezoelectric voltage constant, g, is the electric field generated by a piezoelectric material per unit of mechanical stress applied or, it is the mechanical strain generated in a piezoelectric material per unit of electric displacement applied. The first subscript to g indicates the direction of the electric field generated in the material and the second subscript is the direction of the applied stress or the induced strain, respectively.

g_{33}: Induced electric field in direction 3 (parallel to direction in which ceramic element is polarized) per unit stress applied in direction 3 or induced strain in direction 3 per unit electric displacement applied in direction 3

g_{31}: Induced electric field in direction 3 (parallel to direction in which ceramic element is polarized) per unit stress applied in direction 1 (perpendicular to

direction in which ceramic element is polarized) or induced strain in direction 1 per unit electric displacement applied in direction 3

g_{15}: Induced electric field in direction 1 (perpendicular to direction in which ceramic element is polarized) per unit shear stress applied about direction 2 (direction 2 perpendicular to direction in which ceramic element is polarized) or induced shear strain about direction 2 per unit electric displacement applied in direction 1

Permittivity, ξ: The permittivity, or dielectric constant, ξ, for a piezoelectric ceramic material is the dielectric displacement per unit electric field. ξ^{T} is the permittivity at constant stress, ξ^{S} is the permittivity at constant strain. The first subscript to ξ indicates the direction of the dielectric displacement; the second is the direction of the electric field.

Relative dielectric constant, K: It is the ratio of the amount of charge that an element constructed from the ceramic material can store, relative to the absolute dielectric constant, 0, the charge that can be stored by the same electrodes when separated by a vacuum, at equal voltage (0 = 8.85 x 10-12 farad / meter).

Elastic compliance, s: It is the strain produced in a piezoelectric material per unit of stress applied and, for the 11 and 33 directions, is the reciprocal of the modulus of elasticity (Young's modulus, Y). Here s^D is the compliance under a constant electric displacement and s^E is the compliance under a constant electric field. The first subscript denotes the direction of strain; the second is the direction of stress.

s^E_{11}: elastic compliance for stress in direction 1 (perpendicular to direction in which ceramic element is polarized) and accompanying strain in direction 1, under constant electric field (short circuit)

s^D_{33}: elastic compliance for stress in direction 3 (parallel to direction in which ceramic element is polarized) and accompanying strain in direction 3, under constant electric displacement (open circuit)

2.2.3 Polarization of piezoelectric crystal

The direction of positive polarization generally is along with the Z-axis of a global coordinate system of X, Y, and Z axes. Direction X, Y, or Z is represented by the subscript 1, 2, or 3, respectively, and shear about one of these axes is represented by the subscript 4, 5, or 6, respectively.

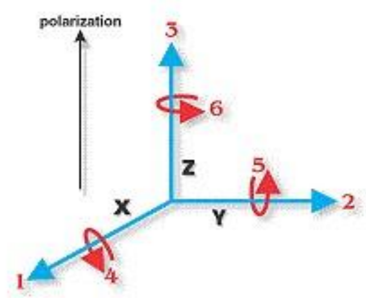

Figure 2.3 Polarization of piezoelectric crystal.

2.3 Piezoelectric structures available for transverse bending

There are different structures like beams, diaphragm, cantilevers are most commonly used for piezoelectric actuation. Among them cantilever is most preferable for sensors, transducers, switches and relays. There are different types of piezoelectric cantilever structures which are multilayer (stack), unimorph, and bimorph, cylindrical.

The actuation of piezoelectric cantilever is most commonly achieved by transforming longitudinal stress within the piezoelectric active layer into a bending moment by depositing or bonding the active piezoelectric layer onto a passive elastic substrate. When an electric field (E_3) is applied across the thickness of the piezoelectric film, a longitudinal strain (S_1) is generated within the film through the transverse d_{31} coupling coefficient following the constitutive relationship given by

$S_1 = d_{31}E_3$ ………...…………………………………………………. (3)

With one surface of the piezoelectric layer constrained by strain matching to the coupled elastic layer, the longitudinal strain is converted into a bending moment due to the offset between the piezoelectric layer and the overall neutral axis of the composite structure, resulting in the displacement of the beam transverse to its length axis. This design configuration, sometimes termed a unimorph or heterogeneous bimorph [20], [21].

Some of the important structures used in micro-actuators are as follows:

2.3.1 Piezoelectric unimorph

It is a cantilever that consists of one piezoelectric layer (active layer) and one substrate layer (inactive layer). The potential applied to active layer produces a strain in that layer but, this strain in opposed by the passive layer cause the induction of opposite strain in that inactive layer. This induction of different strain cause the cantilever beam to employ transverse bending actuation.

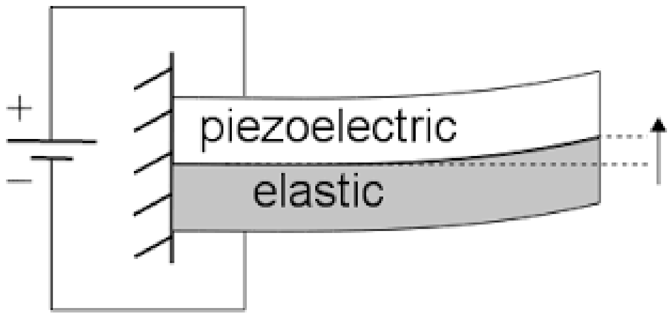

Figure 2.4 Piezoelectric Unimorph. [22]

2.3.2 Piezoelectric Bimorph

A bimorph consists of two identical piezoelectric elements stacked on top of each other (parallel or series arrangement), this layer produces displacement via:

i. Thermal activation (a temperature change causes one layer to expand more than another). ii. Electrical activation as in a piezoelectric bimorph (electric field causes one layer to expand and other layer to contract) this results in a bending deformation.

Like unimorph the bimorph are also used as transducer, pressure measuring system, and energy harvester.

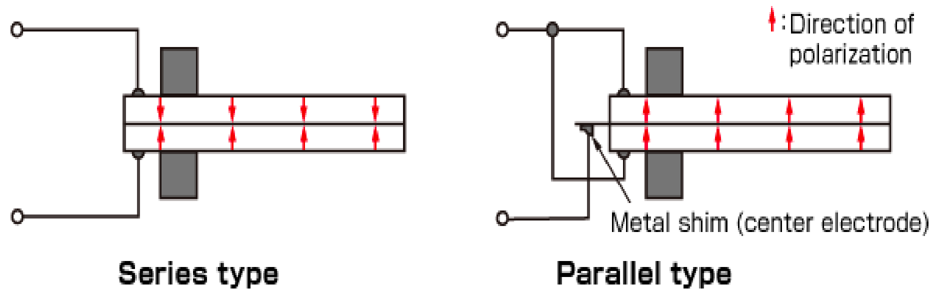

Figure 2.5 Piezoelectric Bimorph. [22]

2.3.3 Homogeneous Transverse Bending mode

Though unimorph and bimorph has been used for a wide variety of actuators, heterogeneous bimorphs present several disadvantages for MEMS systems actuation. First, a composite structure required consisting of both piezoelectric and elastic layers is complicating device fabrication. Applying an electric field through the thickness of the piezoelectric film also requires electrodes on both upper and lower surfaces of the piezoelectric layer. Making electrical contact to a buried electrode between the piezoelectric film and coupled elastic layer further complicates device fabrication. The microfabrication of heterogeneous bimorphs capable of transverse actuation often requires a bonding or adhesive film to mate the piezoelectric and elastic layers, further complicating device fabrication and potentially introducing unwanted damping or strain release into the structure. Finally, from the perspective of electromechanical coupling, the use of transverse-mode $d31$ actuation sacrifices device performance, since $d31$ is typically two to three times smaller than the longitudinal $d33$ coupling coefficient [22].

Hareesh et. al. [15] report a new design topology for piezoelectric heterogeneous bimorph micro-actuators capable of generating transverse bending-mode actuation using a single homogeneous layer of bulk PZT. When, an actuation voltage applied between the electrodes generates field lines parallel to the fixed dipoles, resulting in longitudinal strain ($S3$) though the $d33$ converse piezoelectric effect as

$$S_3 = d_{33}E_3 \quad \text{……………………………………………………} \quad (4)$$

By choosing an appropriate spacing between the interdigitated electrodes, the effective penetration depth of the electric field lines, shown in Fig. 1(b), can be designed to yield a desired offset between the mean strain axis and the location of the beam's neutral axis. Just as with a heterogeneous bimorph fabricated from a coupled piezoelectric/elastic composite structure, this offset converts longitudinal stress into a bending moment within the homogeneous beam, resulting in the desired transverse deflection.

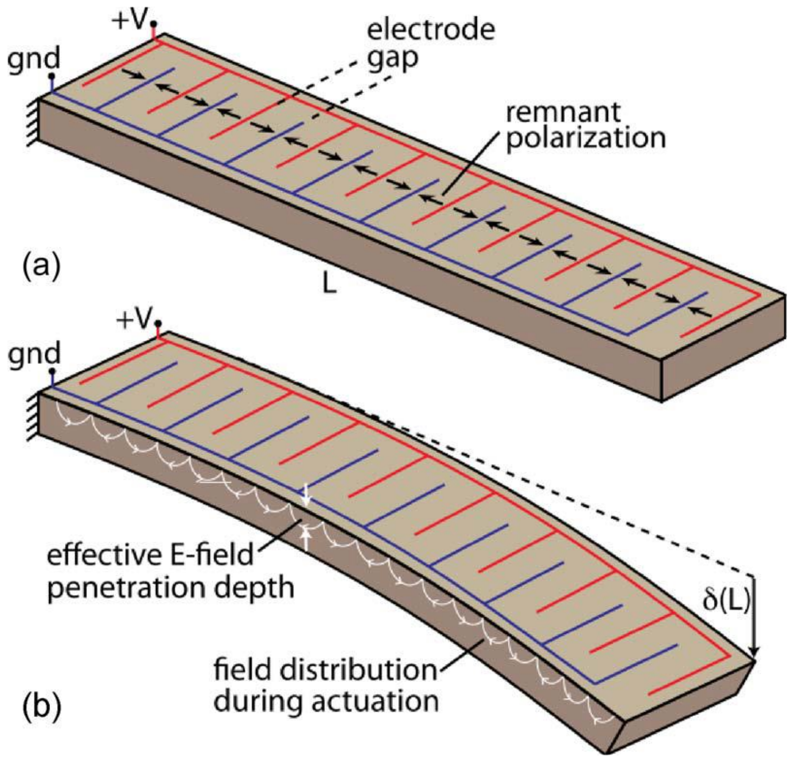

Figure 2.6 (a) Poling and (b) actuation of a homogenous PZT beam using the IDE scheme. [15]

2.4 Various Piezoelectric micro-stages available

The micro-stages that are studied in the past research can be classified according to the degrees of freedom (DOF) they possessed. DOF is the number of independent parameters that define configuration, they are important in the analysis of systems. DOF means how many variables are required to determine position of a mechanism in space.

Youngjoo Yee et. al. [23], proposed micromirror actuated by piezoelectric cantilevered unimorphs. They have reported that by using Metal/PZT/metal thin film actuators how to move an integrated micro-mirror in vertical direction. The device fabricated only provide translation along Z axis and so, only have 1 DOF. They have described preliminary characteristics of PZT, which is deposited using sol-gel method, actuated mirror (PAM) and they have also given fabrication process for the manufacturing of PAM. The critical thing is to decide material for electrodes due to the leakage current, the bonding with the PZT, and the residual stress. They have selected platinum and ruthenium oxide (RuO2) as the bottom and the top electrode. The micromirror can be easily actuated up to several micro-meters under low voltage operation condition well below 10 V.

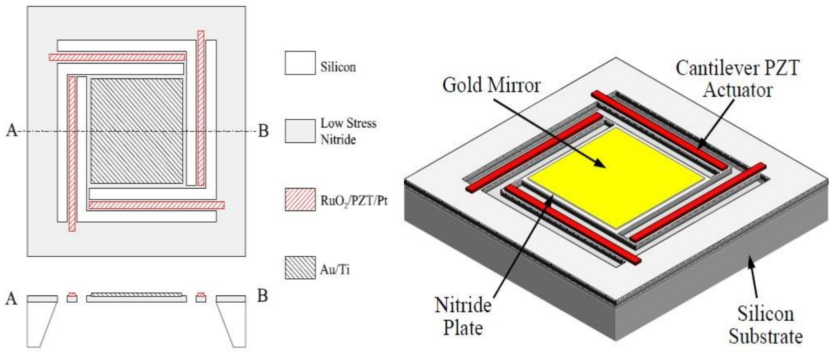

Figure 2.7 Three-dimensional schematic of the PZT actuated micromirror for Nano-steering of the laser beam. [23]

Takayuki Naono et al. [24], have developed design and characteristics of a non-resonant 2-D piezoelectric MEMS scanner actuated by a Nb doped PZT (PNZT) thin film for endoscopic optical coherence tomography (E-OCT). They have used a gimbal-less scanner with folded L-shape actuators enabling two-axis scan motion of a 1 mm x 1 mm mirror within a compact device size of 2.2 mm x 2.7 mm. They have shown that the unimorphs made of PNZT produces more than double displacement as compared to the non- doped PZT films and is suitable for large angle non-resonance scan, which was difficult for conventional non-resonant piezoelectric scanners. Finite element analysis (FEA) of model was performed. They have arrived at conclusion that fabricated MEMS scanner with PNZT actuators showed an optical scan angle of 18.6◦ for both scan axes at a drive voltage of 40 V_{pp} in non-resonance mode. This scan angle is nearly double than that of the scanner with PZT actuators.

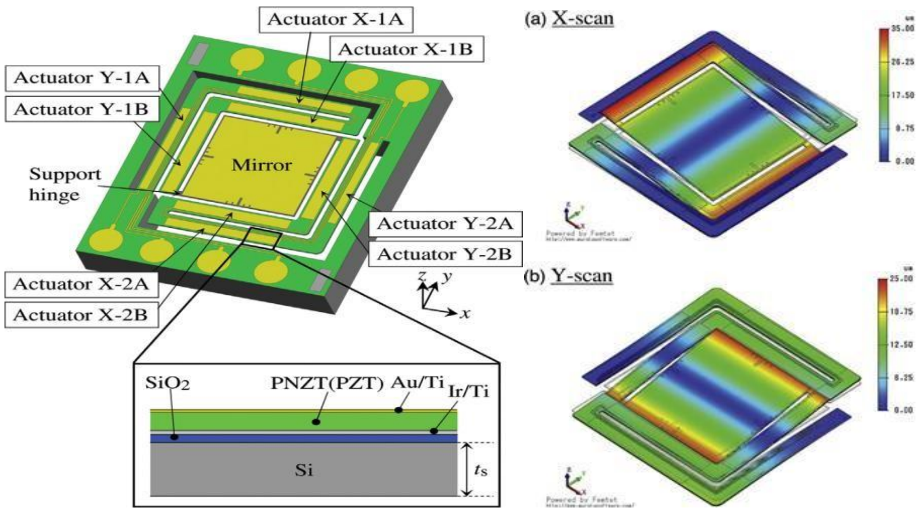

Figure 2.8 Schematic drawing of the piezoelectric 2-D MEMS scanner with L-shape actuators. [25]

E.E.Aktakka et al. [14], have performed the simulation, fabrication and characterization of a 3-DOF piezoelectric micro vibratory stage. They have used vibratory stage in which they utilize four piezoelectric crab-leg suspensions formed of bulk-PZT/Si unimorph beams in an L-shaped layout. In this research, they mainly focused on large X/Y tilting and Z translational motion capabilities of micro-stage. They have done FEA simulations for optimizing the PZT/Si thickness ratio and characterize the 3-DOF actuation modes and off axis coupling. They fabricated device with the help of bonding, lapping and wet-etch patterning of high-quality bulk-PZT films on silicon. The fabricated stage is tested via an optical interferometer to determine its translational and tilting displacement ranges while excited statically with ±25 V_{DC}.

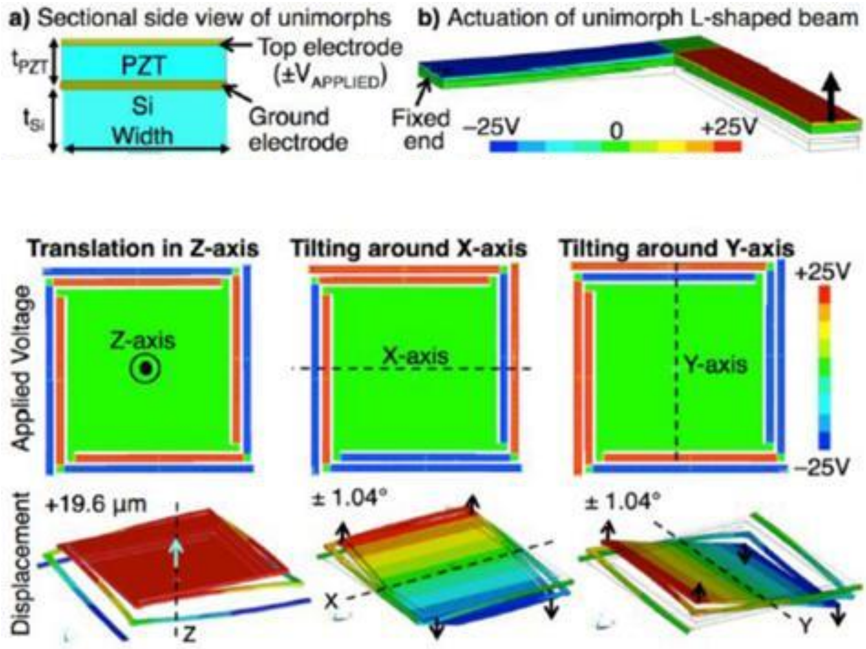

Figure 2.9 Operation principle of the L-shaped PZT beams [14]

2.5 Merits of IDE over PPE

To exploit different piezoelectric coefficient during the actuation mode the pattern and electrode geometry plays a crucial role. Parallel Plate electrode (PPE) is generally used because of their simplicity and ease in patterning however, the device fabrication is complex and the actuation is also comparatively less because of the d_{31} actuation mode. On the other hand, Interdigitated electrode (IDE) provides the utilisation of d_{33} actuation mode to provide more actuation but are comparatively complex to pattern.

IDE facilitates the use of geometrical optimisation to varying the results on the same electrode pattern area which is not possible in care of PPE. Also, they are patterned over a single surface of the device making it easier for probing and characterisation on the other open surface, this may get a bit difficult with the PPE.

Various studies carried out in the past showing the actuation of cantilever actuator using IDE and their comparison with PPE has been done both in simulation and experimentation [16], [25]. The parameter of IDE can be optimised to get the desired result output. This property of IDE further enhances their utilisation to employ the various transduction and actuation of different device structures.

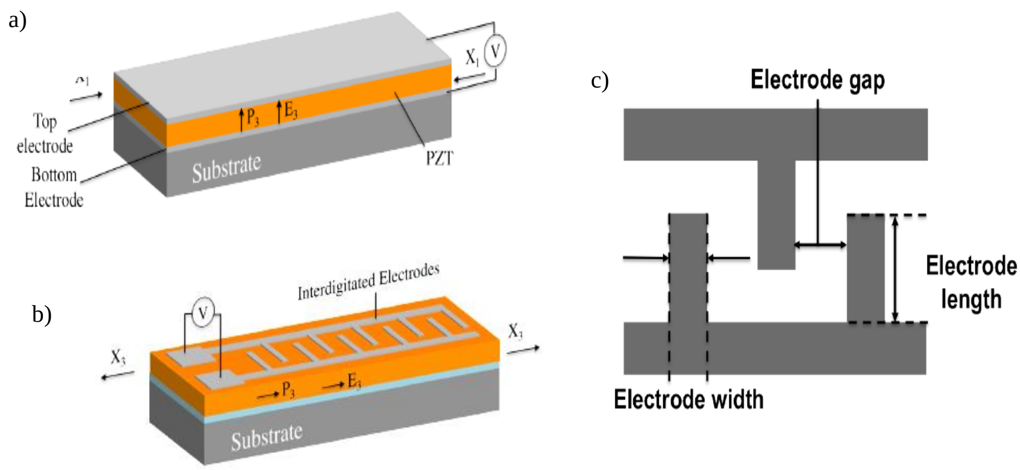

Figure 2.10 A schematic diagram of a cantilever actuated by (a) Parallel Plate Electrode in d31 mode and (b) Interdigitated Electrode in d33 mode (c) Parameterized interdigitated electrodes geometry [25].

Mazzzalai et. al. [26], reports on conception, simulation, and fabrication of a lead zirconate titanate (PZT) MEMS cantilevers for piezoelectric energy harvesting (EH). They investigate the advantages of interdigitated electrode configurations (IDE) with respect to parallel-plate electrodes (PPE) in terms of output voltage and output power from the constitutive equations of piezoelectricity. In their research the shows the benchmarking of different systems for energy harvesting applications through the comparison of the output power for a given input for unit volume. In order to compare the potentialities of both IDE and PPE systems they define the figure of merit for energy harvesting as the product between the effective coefficients d_{ij} and c_{ij}, which has the units of energy per unit volume for a given strain. Calling "*a*" the electrode gap and "*b*" the electrode width we can correct the FOM by the geometrical factor *a/(a+b)* which takes into account the fact that not the whole volume of IDE structures can be exploited.

They deduced the following equation:

$$\frac{FOM_{IDE}}{FOM_{PPE}} = \frac{(d.c)_{IDE}}{(d.c)_{PPE}} \cdot \frac{a}{a+b} = 2.12\frac{a}{a+b} \qquad \ldots\ldots\ldots\ldots\ldots\ldots\ldots (5)$$

The 2.12 factor has been obtained by inserting the piezoelectric and stiffness constant, for a *b/a* ratio which goes from 2 to 10 we expect therefore an energy harvesting performance from 1.4 to 2 times better for IDE structures respect to PPE ones.

Chidambaram et. al. [16], compared both PPE and IDE based Lead zirconate titanate (PZT) thin films on insulator-buffered silicon substrates energy harvester with respect to dielectric, ferroelectric, and piezoelectric properties, leakage currents, and figure of merit (FOM) for energy harvesting. Both films were obtained by an identical sol-gel method. They reported that the dielectric loss was smaller in the IDE case with a higher saturation polarization, a higher coercive field, and less back-switching. The leakage current density of the IDE structure was 4 orders of magnitude lower than that of the PPE structure. The best FOM of the IDE structures was 23% superior to that of the PPE structures while also having a voltage response that was ten times higher.

Brckert and Kreher [27], have done the Finite element Analysis (FEA) of bulk and composite PZT actuator using IDE. They studied the effect of IDE geometry and optimized the product for performance and failure hazard. According to them, the zone between every pair of electrode fingers may be subdivided in three different regions:

(a) an active zone between the electrodes with homogeneous fields, being the source of the module overall deformation,

(b) an ineffective zone in the range beneath the fingers with vanishing fields, responsible for loss of performance,

(c) a transition zone in the range between (a) and (b), with strong field concentrations, acting as possible sources for premature failure.

The balance between these zones is controlled by the geometric parameters of the electrode design. Furthermore, it is dependent on the material properties of the piezoelectric layer. An optimum design should provide a compromise combining and high piezoelectric performance (effective deformation) with a sustainable failure hazard due to local field concentrations during operation.

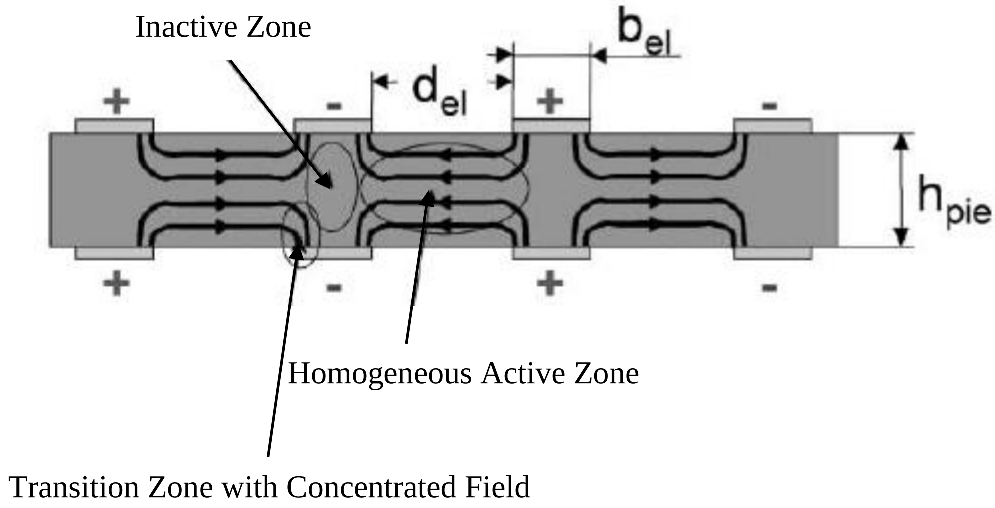

Figure 2.11 Vertical section of an IDE actuator, qualitatively illustrating the distribution of the electric field lines and Transition zones. [27]

2.6 Micro-fabrication techniques

In this section, various micro-fabrication techniques that has been utilised to fabricate various piezo stages has been discussed. The application of stage, its design and material greatly dominates the selection of fabrication techniques. Selection of microfabrication technique depends on the parameters likes overall dimension of product, local features of components, capabilities of material, mass production capability, manufacturing cost. According to the type of energy used for the development, microfabrication techniques can be classified as mechanical, chemical, electrochemical, electrical and laser techniques. UV lithography technique is used for fabrication of electrode pattern on piezo plates due to its advantage over other methods which are discussed latter in this chapter.

2.6.1 Wet Etching

Wet-etching of PZT structures is highly desirable, since it provides a cost-effective, high- throughput process, and enables lithographically-defined features. E.E.Aktakka et. al. [28] presents a new micro-fabrication technique for wafer-level lapping and wet etch patterning of PZT over silicon substrate. The thickness of film can be controlled precisely upto 100 μm with a lapping rate of 10-30 μm/min. They develop a new wet etchant for PZT which can produce low undercuts (0.6:1). To minimize undercut, multiple cycles of lithography followed by wet-etching are used. Only a portion of the total thickness is etched in each cycle (etch rate 2-3 μm/min), followed by ultrasonic cleaning. In their work a new mixture is utilized, BHF:HNO3(67%):HCl(38%) with 2:2:1 ratio, which is 14× diluted by DI-H2O to achieve a controllable etch rate and prevent photoresist-mask delamination. The solution is heated to 40°C in order to increase etching efficiency and obtain a better undercut profile. The etch process is

$$Pb(Ti,Zr)O_3\,(s) + HCL\,(aq) + HF(aq) \longrightarrow [TiF_6]^{2-}(aq) + [ZrF_6]^{2-}(aq) + [PbCl_4]^{2-}(aq) + PbClF(s) + H_2O(l) \quad \ldots\ldots\ldots\ldots (6)$$

$$PbClF(s) + HNO_3(aq) \longrightarrow PbCl_2(s) + Pb^{2+}\,(aq) + NO_3^{-}(aq) + HF(aq) \quad \ldots\ldots\ldots\ldots\ldots\ldots\ldots\ldots (7)$$

where PbClF residue is converted into PbCl2, which has a higher solubility in water.

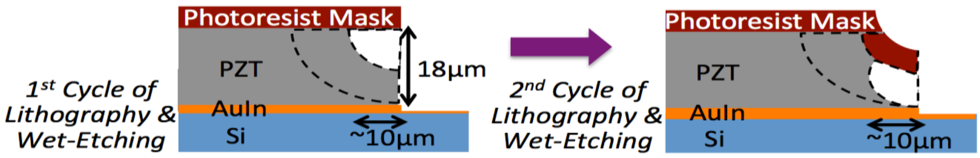

Figure 2.12 Diagram of multi-step wet-etching process.[28]

2.6.2. Deep Reactive-Ion Etching (DRIE)

Deep reactive-ion etching (DRIE) is a highly anisotropic etch process used to create deep penetration, steep-sided holes and trenches in wafers/substrates, typically with high aspect ratios.

Zhang et. al. [29] investigated an inductive coupled plasma (ICP) based DRIE of PZT ceramics. The experimental procedure includes thick photoresist patterned lithography, Ni hard mask electroplating and ICP enhanced deep reactive ion etching using chlorine gas. PZT ceramic pillars with a height of 43.78 μm and a side wall angle of 78.91 were obtained. The optimized etching parameters for PZT ceramics were etching rate of 6.25 μm/h, and PZT/Ni etching selection ratio of 6.9. They optimised the parameters like RF power, Gas Ratio and Chamber pressure to get the desired etching rate. The etching depth and profile angle were 43.78 μm and 78.91 for PZT ceramic.

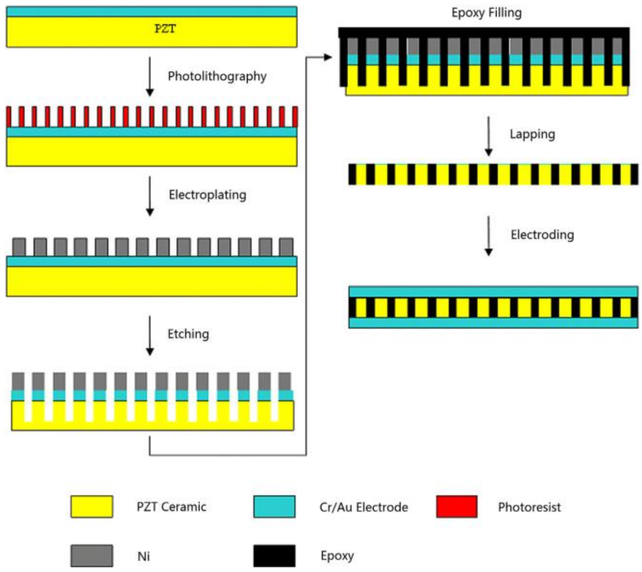

Figure 2.14 Schematic diagram of the micromachining procedure using DRIE.

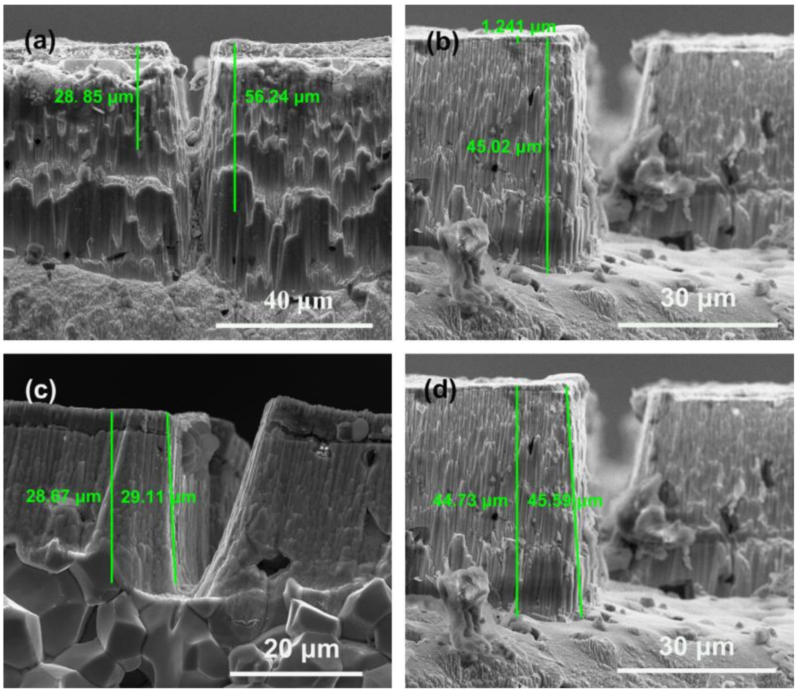

Figure 2.13 SEM cross-sectional morphologies of PZT after etching for 7h. (a) at the original edge of the sample, (b) at the position where the neighbouring element was absent, (c) a newly broken sample, and (d) the morphology for calculation of the side wall angle. [29]

Bale and Palmer [9] employed Reactive ion etching with sulphur hexafluoride (SF6) gas to create deep structures in bulk samples of the piezoelectric material lead zirconate titanate, $Pb(Zr,Ti)O_3$ (PZT). SF6 is chosen for compatibility with dry etching of silicon with a possibility for production of hybrid silicon-piezoelectric devices. Thick photoresist layers have been used to pattern PZT to a depth of 2 mm at a rate of 120 nm-min^{-1}. The use of more durable nickel masks, formed by electroplating through the thick resist, leads to structures greater than 100 mm in height, with an average sidewall angle of ~72°.They also investigated addition of both argon and nitrogen to the SF_6 gas and shown to improve sidewall angles along with heating of the substrate PZT etch rates up to 200 nm-min^{-1} have been obtained.

Wang et. al. [30] in his research shows a deep reactive ion etching (RIE) technique that uses sulphur hexafluoride (SF_6) gas. The etching was performed by using an inductively coupled plasma that was generated in a narrow-gap vacuum chamber. The etch depth was 70 μm with a maximum etch rate of 0.3 μm/min and a selectivity of PZT to the electroplated nickel mask of >35:1. The sidewalls of the PZT structures were tapered, with base angles of ~75°. They also discussed that the reaction products from the reaction of SF_6 with PZT, such as PbF_2, TiF_4, and ZrF_4, have high vaporization points and barely volatize at room temperature, even under reduced pressures. Once deposited on the PZT surface, reaction products may remain there, to prevent further PZT etching, and therefore decrease the etch rate, as well as the sidewall verticality. Thus far, SF_6 rarely has been used in RIE of PZT.

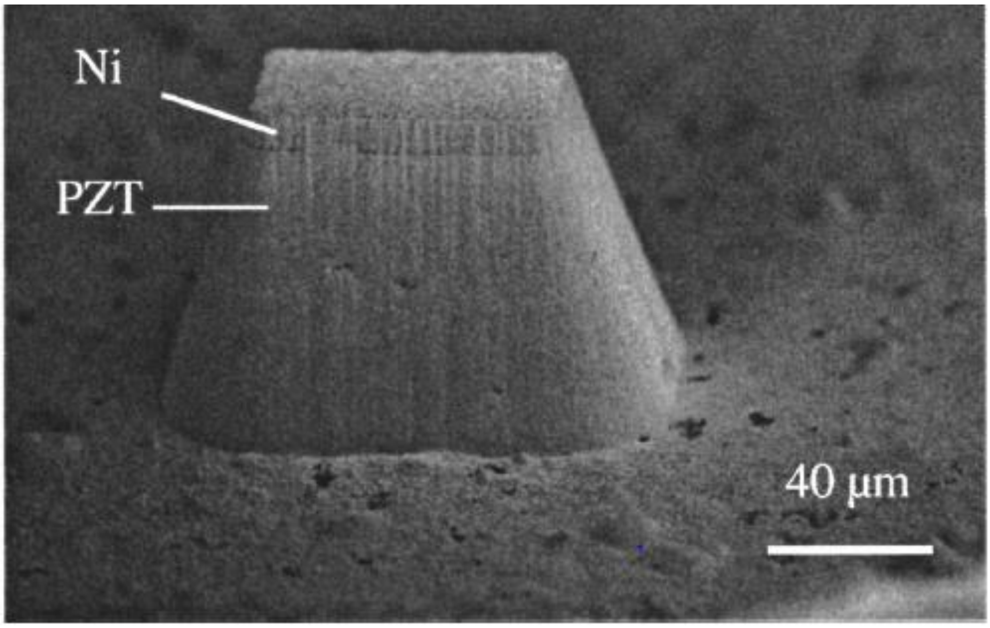

Figure 2.15 PZT structures fabricated by deep RIE process, close-up of a PZT rod; the top white layer indicates the remaining portion of the nickel mask. [30]

2.6.3 Ultrasonic Machining

Ultrasonic machining, or strictly speaking "Ultrasonic vibration machining", is a subtraction manufacturing process that removes material from the surface of a part through high frequency, low amplitude vibrations of a tool against the material surface in the presence of fine abrasive particles. The tool travels vertically or orthogonal to the surface of the part at very low amplitudes. The fine abrasive grains are mixed with water to form a slurry that is distributed across the part and the tip of the tool.

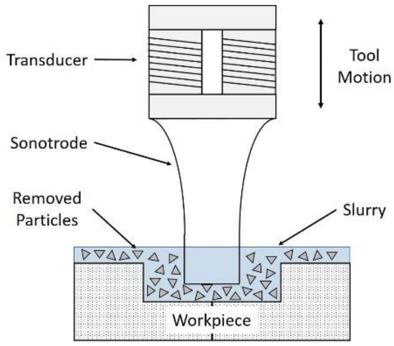

Figure 2.16 Schematic of ultrasonic machining process.

Li and Gianchandani [11] developed a new fabrication process which combines lithography, electroplating, batch mode electronic discharge machining (EDM) and batch mode ultra-sonic machining (USM) to provide die-scale pattern transfer capability from lithographic mask onto ceramics, especially piezoceramics like PZT etc. A die-scale pattern with 25 μm minimum feature sizes was defined with a mask and transferred onto the workpiece with a machining speed of 18 μm/min. As a demonstration, an octagonal spiral shape in-plane actuator with footprint of 450 μm x 420 μm and wall width of 50 μm was fabricated on bulk PZT.

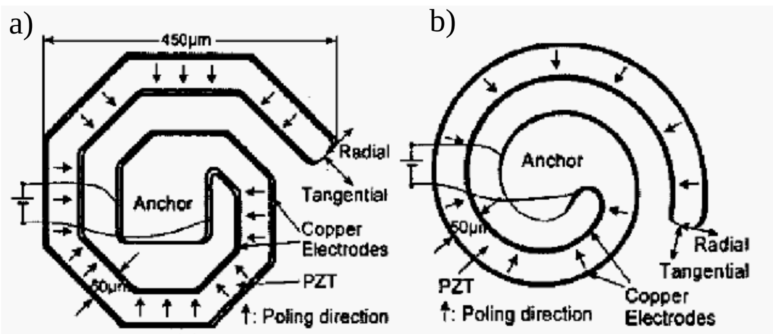

Figure 2.17 Schematic of: (a) octagonal spiral actuator; (b) circular spiral actuator. The short arrows indicate poling direction along the spiral. [11]

2.6.4 Micro Powder Blasting Technique

Misri et. al.[13] presented a facile fabrication process for bulk PZT microsystems using dry film photoresist and micro powder blasting. The combination of dry film photoresist masking and powder blasting using micron-scale alumina particles provides a powerful and simple process for the microfabrication of transducers from high-performance bulk piezoelectric materials. They evaluated the optimum etching characteristics by using mask features ranging from 25µmto 150µm, PZT and dry film photoresist, with results indicating the use of larger particles at low nozzle pressure and small nozzle distance to achieve an optimal range of etch rate, etch selectivity and anisotropy in the resulting etch. The etching process has been used to successfully fabricate piezoelectric cantilever micro actuators based on d33 unimorph and d31 multimorph topologies, in the former case using a single layer of PZT with thin film interdigitated electrodes patterned on one side of the piezoelectric substrate, and in the latter case employing a composite PZT/glass structure.

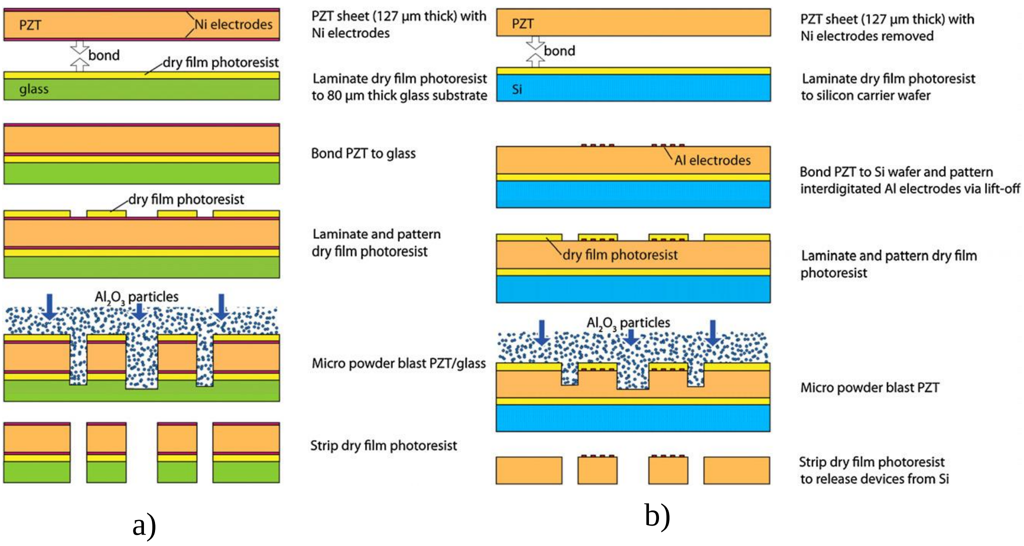

Figure 2.18 Overview of the bulk PZT cantilever microfabrication processes for (a) d31 mode PZT/glass multimorph and (b) d33 mode PZT [13].

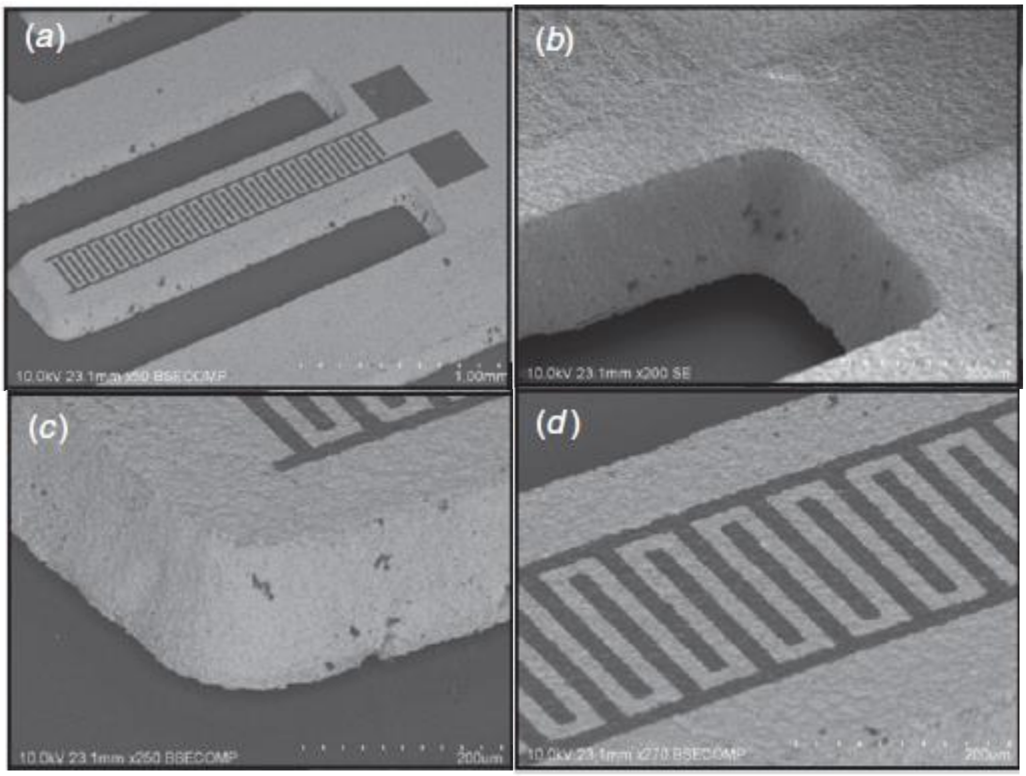

Figure 2.19 (a) Electron micrograph of a d33 unimorph cantilever, with magnified views of (b) inside and (c) outside corners of the cantilever structure patterned by micro powder blasting. (d) Detailed image of the interdigitated electrodes with 20 µm spacing. [13]

2.6.5 Abrasive Water Jet Machining (AWJM)

Water Jet Machining (WJM) and Abrasive Water Jet Machining (AWJM) are two non-traditional or non-conventional machining processes. They belong to mechanical group of non-conventional processes like Ultrasonic Machining (USM) and Abrasive Jet Machining (AJM). In these processes (WJM and AJWM), the mechanical energy of water and abrasive phases are used to achieve material removal or machining. The term abrasive jet refers specifically to the use of a mixture of water and abrasive to cut hard materials such as metal or granite, while the terms pure waterjet and water-only cutting refer to waterjet cutting without the use of added abrasives, often used for softer materials such as wood or rubber. However, in all variants of the processes, the basic methodology remains the same. Water is pumped at a sufficiently high pressure, 200-400 MPa (2000-4000 bar) using intensifier technology. When water at such pressure is issued through a suitable orifice (generally of 0.2- 0.4 mm dia), the potential energy of water is converted into kinetic energy, yielding a high velocity jet (1000 m/s). Such high velocity water jet can machine thin sheets/foils of aluminium, leather, textile, frozen food etc.

In pure WJM, commercially pure water (tap water) is used for machining purpose. However, as the high velocity water jet is discharged from the orifice, the jet tends to entrain atmospheric air and flares out decreasing its cutting ability. Hence, quite often stabilisers (long chain polymers) that hinder the fragmentation of water jet are added to the water.

In AWJM, abrasive particles like sand (SiO2), glass beads are added to the water jet to enhance its cutting ability by many folds. AWJ are mainly of two types – entrained and suspended type as mentioned earlier. In entrained type AWJM, the abrasive particles are allowed to entrain in water jet to form abrasive water jet with significant velocity of 800 m/s. Such high velocity abrasive jet can machine almost any material.

Waterjet cutting is often used during fabrication of machine parts. It is the preferred method when the materials being cut are sensitive to the high temperatures generated by other methods.

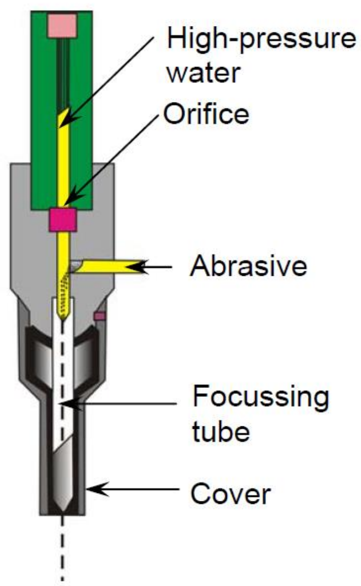

Figure 2.20 Schematic view of the cutting head of AWJM.

2.6.6 Laser Ablation

Zeng et. al. [12] investigates UV laser (λ = 355 nm) ablation of piezoelectric lead zirconate titanate (PZT) ceramics in air under different laser parameters. It has been found that there is a critical pulse number (N = 750). When the pulse number is smaller than the critical value, the ablation rate decreases with increasing pulse number. Beyond the critical value, the ablation rate becomes constant. The ablation rate and concentrations of O, Zr and Ti on the ablated surface increase with the laser fluence, while the Pb concentration decreases due to the selective evaporation of PbO. The loss of the Pb results in the formation of a metastable pyrochlore phase. ZrO2 was detected by XPS in the ablated zone. Also, the concentrations of the pyrochlore phase and ZrO2 increase with increasing laser fluence. The results clearly indicate that the chemical composition and phase structure in the ablated zone strongly depend on the laser fluence. The piezoelectric properties of the cut PZT ceramic samples completely disappear due to the loss of the Pb and the existence of the pyrochlore phase. After these samples were annealed at 1150 ◦C for 1 h in a PbO-controlled atmosphere, their phase structure and piezoelectric properties were recovered again.

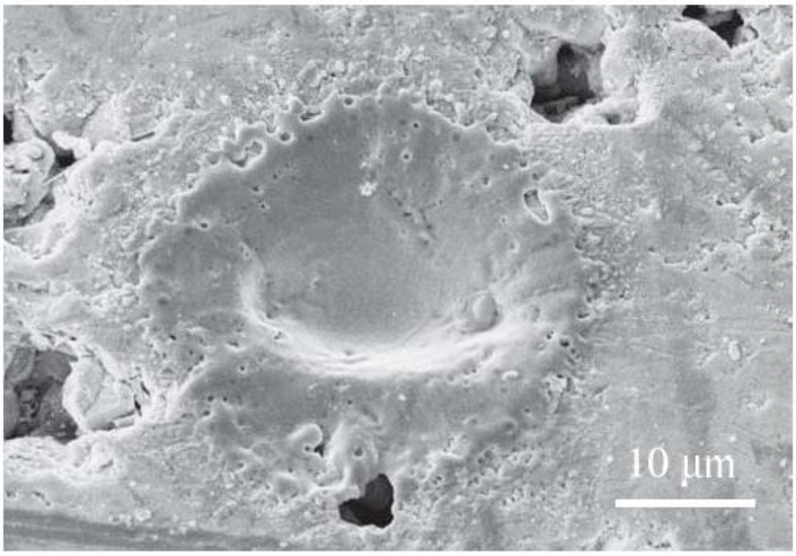

Figure 2.21 The UV pulsed laser-generated crater (ablation conditions: fluence F = 12.7 Jcm−2, N = 5 pulses). [12]

2.6.7 UV Lithography

Lithography is a technique of transferring any desired pattern on to the substrate. Lithography is originated from a Greek word (lithos- stone, Graphein - write). In lithography substrate is subjected to radiations which are filtered by mask.

Advantages of lithography

1. High Aspect Ratio: Aspect ratio (AR) is the ratio of height of device to critical dimension of device, in space.
2. Good accuracy.
3. Produces highly accurate mould inserts for LIGA.
4. Allow one integrated micro-component into single platform
5. Manufacturing cost reduced & reproducibility improves
6. Large material range is used for fabrication

2.6.7.1 UV-Lithography

It is a photolithography technique in which substrate coated with photo sensitive material called photoresist (PR) is exposed to UV light to transfer a 2-D geometric pattern from photomask. Light of particular wavelength (normally in UV region) is passed through transparent region of photomask and is absorbed by photoresist that causes chemical changes in PR. UV exposed PR is kept in the developer to obtain required pattern.

2.6.7.2 UV-mask

Stencil which is used for repetitive generation of desired pattern on photoresist coated wafer is called mask. Mask contains opaque (black dark) and transparent region. Radiations are allowed to pass through transparent region into PR coated substrate, while obstructed by opaque region. According to distance between mask and substrate, masks are classified as (i) direct contact mask, (ii) soft contact mask and (iii) shadow printing mask.

2.6.7.3 Photoresist

Photoresist is photosensitive material. After absorption of radiation of particular wavelength its chemical composition is changes. According to response of PR to light, PR is classified as positive PR and negative PR discussed in Table 2.2.

Table 2.2 Comparison between Positive and Negative photoresist

	Positive PR	**Negative PR**
Figure	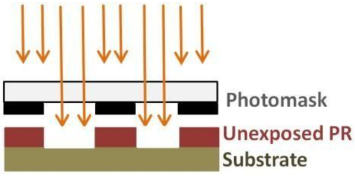	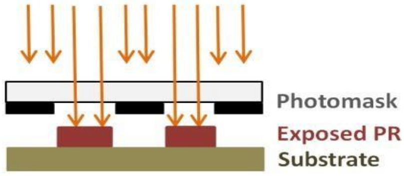
Composition	Photosensitive compound + base resin + organic solution	Photosensitive compound + monomer
Exposure	Brakes polymer chains	Cross-linking of monomer
Development	Expose portion is removed	Exposed portion is remains
Photoresist	AZ, S-1818, PMMA.	SU-8.

2.7 Current Scenario

According to E.E.Aktakka et.al.[31] the present scenario of various stages available with their specification in size, DOF, motion and input energy are shown in Table 2.3 below.

Table 2.3 Current scenario of various multi DOF stages developed using various actuation media. [31]

Actuation Method	**Size of Stage** (mm2)	**DOF**	**Translation motion** (µm)	**Rotational Motion**	**Excitation Input (V)**	**Authors**
Piezoelectric	2 × 2	1	80	N/A	20	Z. Qiu et. al. (2010)
Electrostatic	8 × 8	2	25	N/A	84	J.-C. Chiou et. al. (2010)
Electrostatic	8 × 8	3	18	±1.7°	85	D. Mukhopadhyay et. al. (2008)
Piezoelectric	15 × 15	6	1.5	±0.02°	80	H. Xu et. al. (2006)
Electromagnetic	16 × 16	6	±5	±0.25°	0.3	D. S. Golda et. al.(2008)
Piezoelectric	3 × 3	3^{*} /$6^{\#}$	> ±7.5	> ±0.5°	25	E. E. Aktakka et. al. (2013)

(tested, # simulated)*

Chapter 3

Design of Piezo Stage and Electrode Patterns

3.1 Introduction

In this chapter, the design and simulation of Monolithic Piezoelectric Stage (MPS) is done. MPS is advantageous in gaining precision over its contemporary. For which properties of piezoelectric plates of PZT-5H, dimensions of piezo stage and electrode patterns over piezo stage are important to be discussed. Various other design parameters are also determined by finite element analysis (FEA). The FEA is done using Comsol Multiphysics software.

3.2 Actuation method of Piezo Stage

An unimorph/bimorph gives only 1 DOF i.e. out of plane motion whereas an L-shaped beam when used from all the four sides can deliver out of plane motion with 3 DOF (i.e. uniform tilting along X and Y axes and translation along Z axis) [14]. However, the tilting of stage obtained by constraining four simple cantilever unimorph/bimorph is not symmetric. This symmetry for out of plane tilting can be achieved by using L shaped cantilever unimorph and providing opposite polarity or bending moment to the two legs normal to each other of L shape cantilever beam. Furthermore, the piezoelectric cantilever using PPE can perform out of plane motion only if bonded with a passive substrate resulting in bending moment. The Figure 3.1 shows the idle unimorph/bimorph design and L shaped cantilever design. Following this it is proposed to used such a geometry shown in Figure 3.2[14]. Here, L shaped

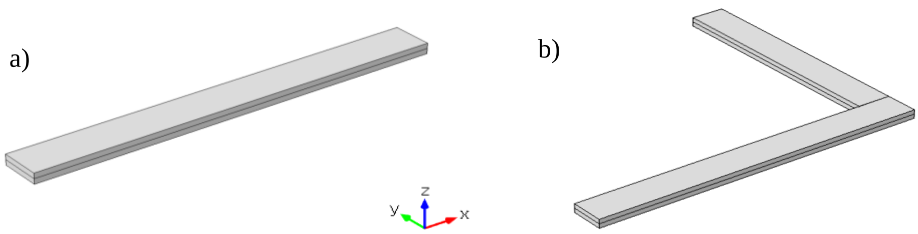

Figure 3.1 a) Unimorph/Bimorph cantilever design b) L shape cantilever Design.

unimorphs are arranged in such a manner where it can deliver uniform tilting motion along with translation.

3.3 Figures of merits of Piezo Stage

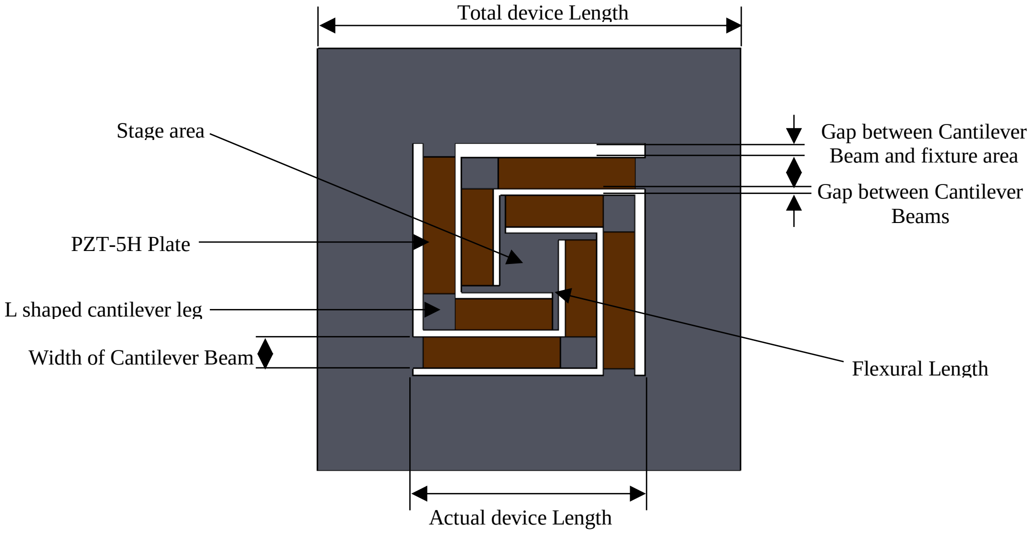

Figure 3.2 Proposed design of Piezo Stage.

Figure 3.2 shows the design parameters on which the performance of piezoelectric stage depends.

3.3.1 Piezoelectric stage size

Foot print of the piezo stage depends on the size of effective piezo stage area/platform, L shaped actuators and the area necessary for mountings. It can be said that larger the L shaped cantilever beams more will be the PZT material requirement. This size provides the sufficient piezoelectric material for getting desired actuation however the size is constrained by the selection of microfabrication techniques available for device fabrication.

3.3.2 Gap between adjacent piezoelectric beams

Gap between adjacent piezoelectric beams plays an important role in stiffness of piezo stage or in other words stiffness of piezo stage inversely proportional to distance between adjacent piezoelectric beams. Moreover, for a given foot print increasing the gap will decrease the piezo actuation and ultimately the overall output.

3.3.3 Flexural Length

The flexural length is very important part of the stage and has great effect on the uniformity (symmetry along axis of tilting motion) of tilting of piezo stage. The dimensions are very carefully taken by doing multiple simulations to minimize the deviation in tilting without affecting the strength of the piezo stage.

3.3.4 Piezoelectric material

The performance of piezo stage is a strong function of the piezoelectric coefficient that is d_{31} and d_{33}. So, we have selected the material to ensure that selected piezoelectric material has larger d_{33} coefficient for better results. The material has been imported from Piezo System, Inc., USA. The plate dimensions are 72.6x72.6 mm^2 having a thickness of 191 μm and about 100-200 nm of Nickle electrode deposited over both surface of the plate. The parameter listed in the Table 3.1 shows the various properties of the piezoelectric material PZT-5H.

Table 3.1 Material Properties of PZT-5H (Piezo System, Inc.)

Material types		**PZT-5H (Piezo System, Inc.)**	**Comsol Multiphysics**
Parameters	**Notation**		
Composition		Lead Zirconate Titanate	
Material Designation		Type 5H4E	
Piezoelectric Charge Constants (pm/V)	d_{33}	650	593
	d_{31}	-320	-274
Piezoelectric voltage constants (mV-m/N)	g_{33}	19	23.24
	g_{31}	-9.5	-6.62
Relative dielectric constants (@1KHz)	K^T_3	3800	-
Polarization Field (V/m)	E_p	$1.5x10^6$	-
Initial Depolarization Field (V/m)	E_c	$3.0x10^5$	-
Elastic constants ($X10^{10}N/m^2$)	Y^E_3	5	-
	Y^E_1	6.2	-
Mechanical Q	Qm	32	-
Curie temperature (°C)	Tc	230	-
Density (Kg/m^3)	p	7800	7500

3.3.5 Electrode Patterns

Electrode patterns used for actuation purpose has been discussed in section 2.3 and their merits has been discussed in section 2.5. PPE uses the d_{31} coefficient of piezoelectric material whereas IDE uses d_{33} coefficient for actuation. The utilization of these coefficients to produce deformation is shown in Appendix A. PPE requires unimorph/bimorph design to produce bending and fabrication of unimorph/bimorph is done by using a bonding agent to bond different layers. This bonding reduces the accuracy and effectiveness of actuator over time because of the introduction of bonding agent. The accuracy, precision and effectiveness can be increased by using IDE on a single layer of piezoelectric cantilever to obtain transverse actuation. So, we propose a new L shaped beam actuated by using IDE over piezo plates. The piezo stage carries four L shaped beams having eight pairs of IDE electrode patterns over it. By utilising this design actuation like translation in Z direction and tilting along X or Y axis can be obtained.

3.4 Modelling of PPE based piezoelectric stage

Keeping the foot print of the device 20x20 mm^2 we have designed new L shaped piezoelectric stage. This stage is able to gives

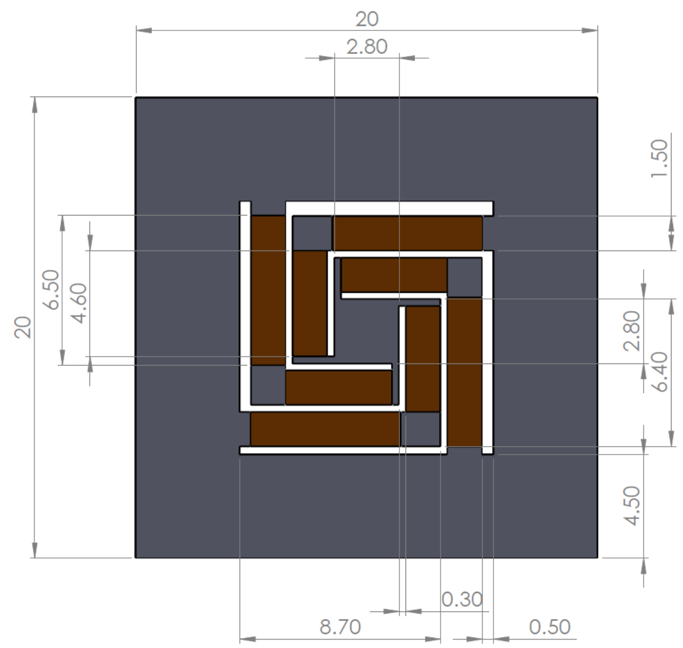

Figure 3.3 Dimensions of PPE based Piezo Stage in mm.

X-tilt, Y-tilt and Z-translation. Modelling of this structure is done on Comsol Multiphysics using dimensions described in the 3-D model of piezoelectric stage Figure 3.3.

The Figure 3.4 shows the piezo stage based on the PPE based model. An unimorph is prepared taking brass of 300 μm thickness as substrate and PZT-5H plates as the active layer of thickness 191 μm. The steps involved in simulation of the piezo stage are described in details in section 3.6.

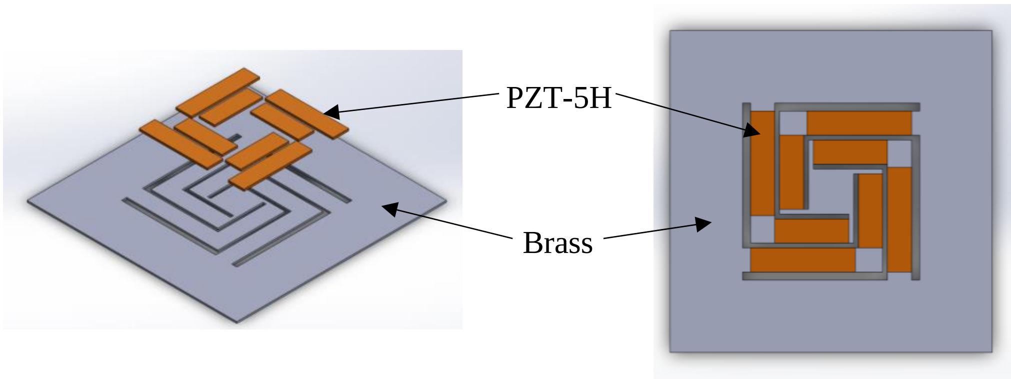

Figure 3.4 a) Exploded vie and b) Planner view of PPE based Unimorph Piezo Stage.

3.4.1 Boundary conditions

The analysis involves piezoelectric material which is electromechanical in nature. Different sets of mechanical and electrical boundary conditions have been used to produce different results. The mechanical boundary conditions are imposed by constraining all displacement of one side of the beam to define a fixed-point case while all other surfaces are free. For the electrical boundary condition, electric potentials are given to the top surface of the actuator where electrodes are made

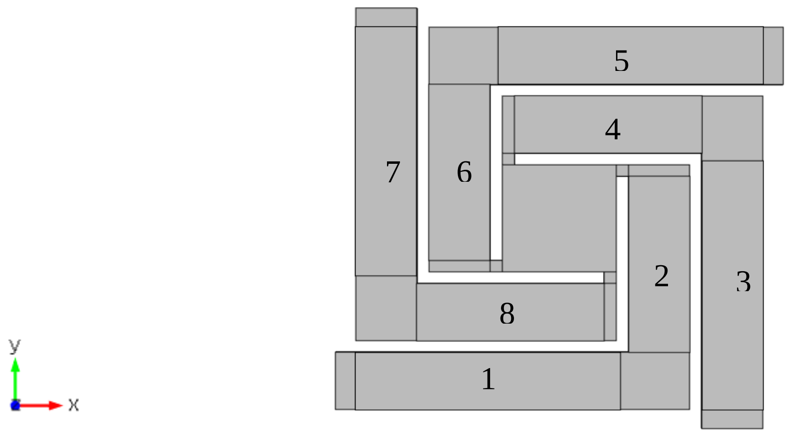

Figure 3.5 Electrode constraints for PPE based Piezo Stage.

and the brass plate is kept grounded. The numbering of electrodes is shown in Figure 3.6 and the electrical constrains are shown in Figure 3.6.

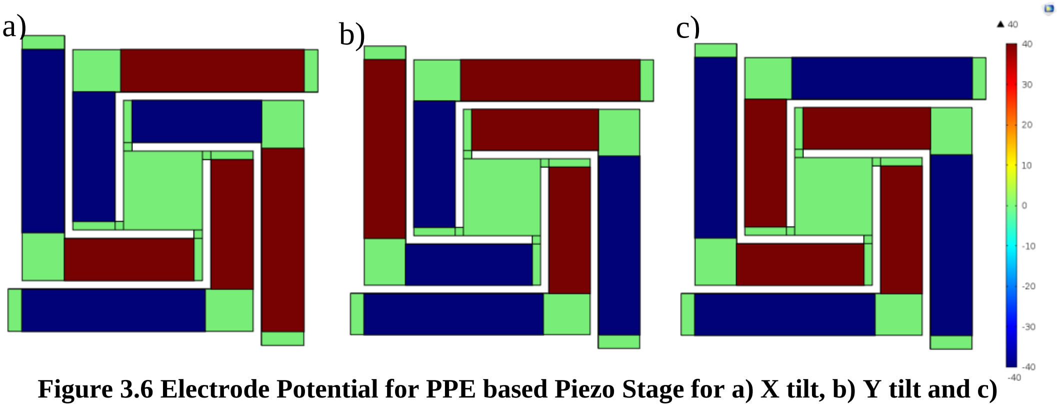

Figure 3.6 Electrode Potential for PPE based Piezo Stage for a) X tilt, b) Y tilt and c) Z translation.

3.4.2 Simulation Results for PPE based Piezo Stage

The deflection of the unimorph/bimorph cantilever and L shaped cantilever is shown in the following Figure 3.7 to represent the symmetric and uniform tilting motion of the stage. The static analysis shows that the piezo stage has been deflected in X, Y, Z directions. Figure 3.8 shows contour plots showing the surface displacement of the piezoelectric stage.

Simulation results in Table 3.2 shows that X Tilt, Y Tilt and Z translation are achieved by this structure with the magnitude of 3.52 (0.14º), 3.52 (0.14º) and 3.05 micrometres respectively for a potential of 40 volts.

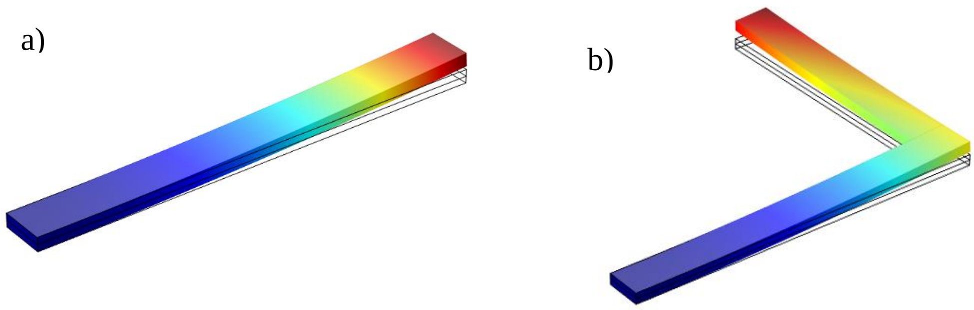

Figure 3.7 Deflection of a) Unimorph/Bimorph and b) L shape cantilever.

Table 3.2 Simulation Results for PPE based Piezo Stage.

SNo,	Actuation	Result
1	X Tilt	3.52 μm (0.14º)
2	Y Tilt	3.52 μm (0.14º)
3	Z translation	3.05 μm

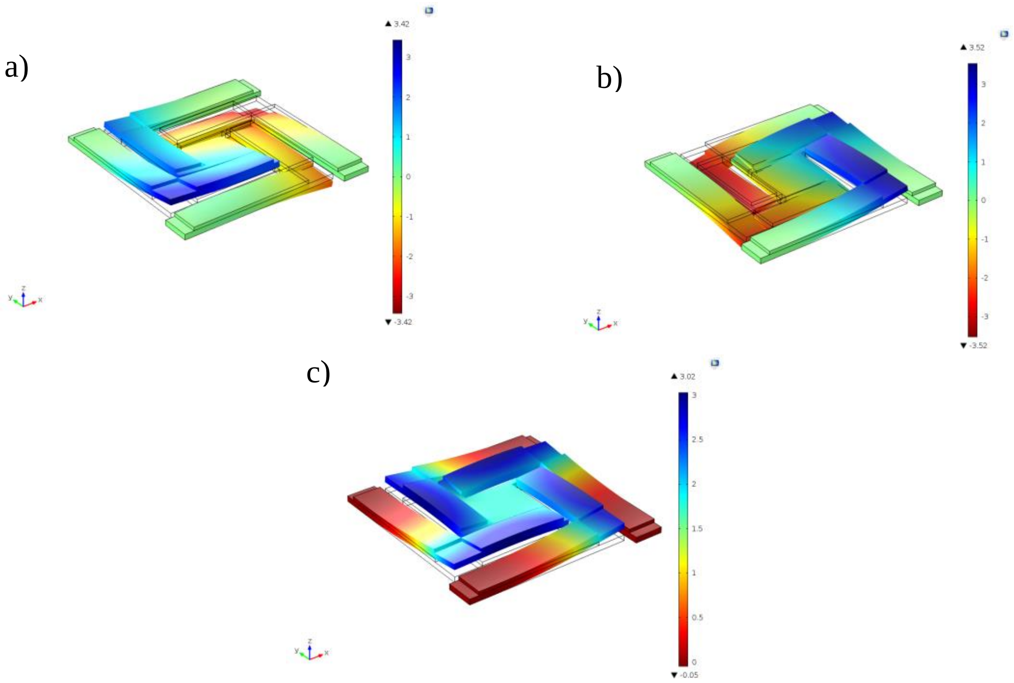

Figure 3.8 Contour plots showing the surface displacement of the piezoelectric stage when actuated at 40 volts DC: (a) X-tilt, (b) Y-tilt and (c) Z-translation.

3.5 Comparison of Electrode Patterns and Geometry

Electrode patterning has been done on both side of all the four L shaped cantilever legs. The IDE patterns has been modelled over the entire length of the beam and the parameters for the IDE geometry has been selected from the optimised result of various simulations carried out using different sets of parameter and geometry.

For the selection of the geometrical and design parameters of IDE various simulation has been done using a simple cantilever of length (L) 4 mm width (W) 0.5 mm and thickness. Both IDE and PPE has been used for the actuation of this cantilever with the potential of 40 volts and the tip deflection is measured and compared for different iterations. The optimum geometrical parametres of IDE are selected form various simultaion results which is discussed in Table 3.3 . The comarison results of simultaion for PPE and IDE actuation mode are dicussed in table 3.4. The Figure 3.9 (a) shows the structure of monolithic cantilever and IDE patterns over it, and Figure 3.9 (b) shows the structre of unimorph/bimorph actuated using PPE.

Table 3.3 Parametric study of IDE patterns for MPS over a cantilever of size 4000x300x150 µm3.

S.No.	Length of Electrode finger (µm)	Width of Electrode finger (µm)	Gap between Electrode finger (µm)	Potential Applied (V)	Deflection of Tip (µm)
1	400	50	200	40	5.82
2	400	50	150	40	7.2
3#	400	50	100	40	9.04
4	400	75	100	40	7.91
5	400	100	100	40	7.74

(# Final parameters used for the comparison of IDE and PPE in Table 3.4)

Table 3.4 Comparison of PPE d31 and IDE d33 actuation mode.

S.No.	Material	Thickness (T)	Type	Electrode Patterns	Deflection of Tip (µm)
1	PZT and Structural Steel	300	Unimorph	PPE	2.5
	PZT and PZT	300	Unimorph	PPE	2.7
			Bimorph	PPE	5.4
4			Unimorph	IDE	1.5
5			Bimorph	IDE	3.1
6	PZT	150	Monolithic	IDE (Single Surface)	4.5
7				IDE (Both Surface)	9

a)

b)

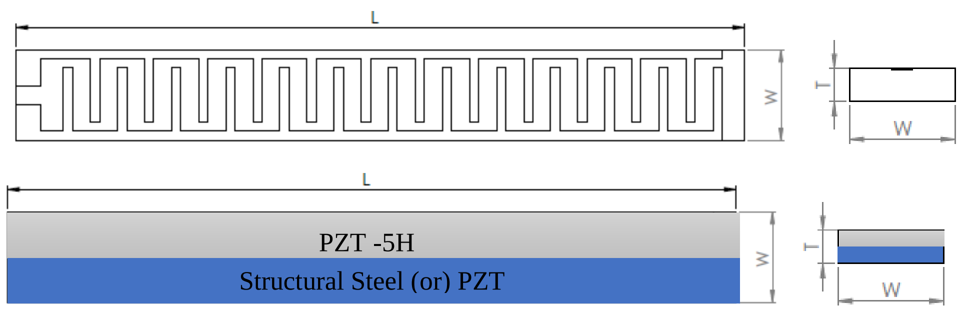

Figure 3.9 Parameter optimisation for a) IDE geometry and comparison with b) PPE geometry.

The contour plots of electric field lines produced during the excitation by PPE and IDE are discussed in Appendix B.

By studying all the parameters for the IDE geometry, the final parameters have been selected as given in Table 3.5. The Figure 3.10 shows the IDE patterns over the MPS:

Table 3.5 Final parameters for IDE geometry.

S. No.	Parameters	Unit (µm)
1	Length of electrode finger	1250
2	Width of electrode finger	50
3	Gap between electrodes	100
4	Thickness of connecting runner	100

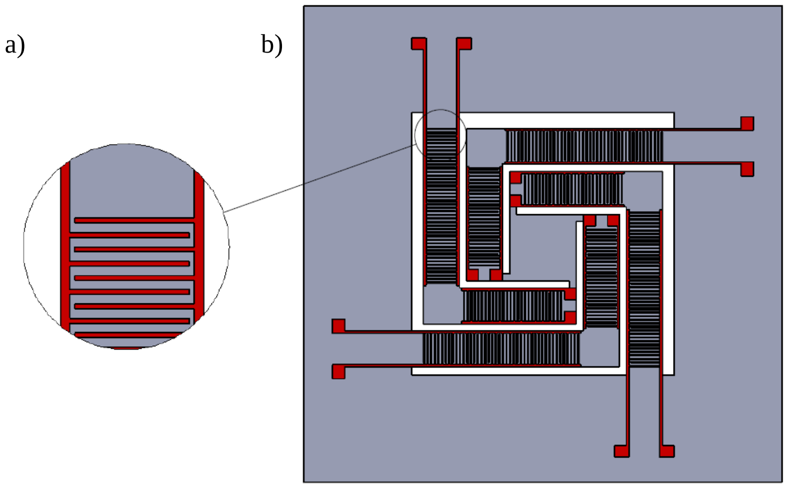

Figure 3.10 a) Detailed view and b) pattern of electrode over the device structure.

3.6 IDE based Monolithic Piezo stage (Modelling in COMSOL)

In this work, Comsol Multiphysics is used as due to its many advantages as robust meshing, auto detection element type, extensive library of material models, powerful solver capabilities, advanced post-processing, etc. over others. In the next section, a vivid discussion is made about the models designed and the structural analysis using Comsol Multiphysics. The inherit property of PZT-5H in this FEA software has a poling direction in Z direction, but for this simulation and analysis work the poling orientation has to be changed according to the electrode geometry to act in d_{33} actuation mode. For this the cantilever is divided into segments and the poling orientation has been defined for each segment.

3.6.1 Add physics

The physics used for this analysis is Structural Mechanics → piezoelectric devices (**pze)**. The Piezoelectric Devices interface combines Solid Mechanics and Electrostatics together with the constitutive relationships required to model piezoelectric devices.

3.6.2 Defining Local Coordinates

Four local coordinates have to be define under the Definition Tab of the Model builder of COMSOL as to define the four poling orientation of the PZT material. This is done by selecting Base Vector Coordinate system in the Definition Tab and defining the parameters as given in the Table 3.6 below:

Table 3.6 Defining the Local Coordinates for Poling direction.

For +X	X	Y	Z
X1	0	0	-1
X2	0	1	0
X3	1	0	0

For -X	X	Y	Z
X1	0	0	1
X2	0	1	0
X3	-1	0	0

For +Y	X	Y	Z
X1	1	0	0
X2	0	0	-1
X3	0	1	0

For -Y	X	Y	Z
X1	1	0	0
X2	0	0	1
X3	0	-1	0

3.6.3 Defining Geometry

In this section, the entire cantilever beam has been divide into small segments between the alternative electrode pairs so as to define the specific poling orientation for each segment. This is done by building the entire

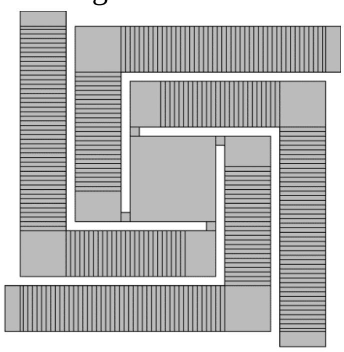

Figure 3.11 Geometrical Model of stage in segmented form build in COMSOL Multiphysics.

geometry in form of small blocks and arrays. Figure 3.11 represents the geometry of MPS

3.6.4 Defining Localized Polarization

With the use of IDE, the polarization between alternative electrode pair changes in direction. This property is not inherited in COMSOL Multiphysics so we have to define the local polarization between each pair of electrode to facilitate the desired actuation.

This is done under the Solid Mechanics tab of the Model Builder. We have selected four Piezoelectric material domains and assign the local coordinates for each of them described in Table 3.6 to define the polarization direction.

Figure 3.12 shows the selection of segments for defining poling direction:

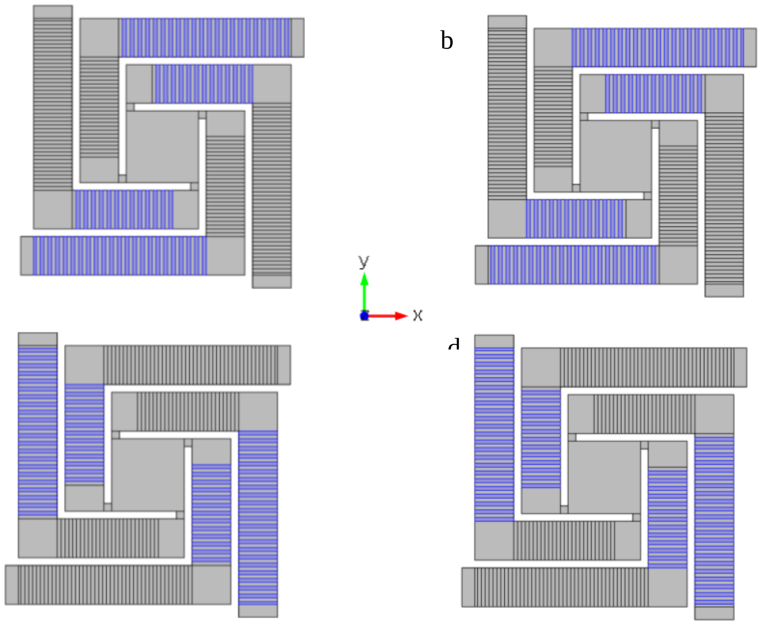

Figure 3.12 Figure showing the polarization vector of segments oriented in a) +X, b) -X, c) +Y and d) -Y directions.

3.6.5 Electrode Patterns

After the segmentation and of geometry and defining all the polarization directions for those segments the electrode geometry has been patterned over both the sides of the piezo stage. The dimensions of the electrode geometry have been selected from the various simulation results listed in Table 3.5. Figure 3.13 shows the IDE pattern over both the surface of the stage. Total 16 pairs of electrode is patterned over the four cantilever legs and the numbering scheme is also mentioned in the Figure 3.13. The finger of the electrode has been patterend in such a way that each finger shares two segments of the cantilever in equal proportion so as to use the electric field gradient according to the poling dirction.

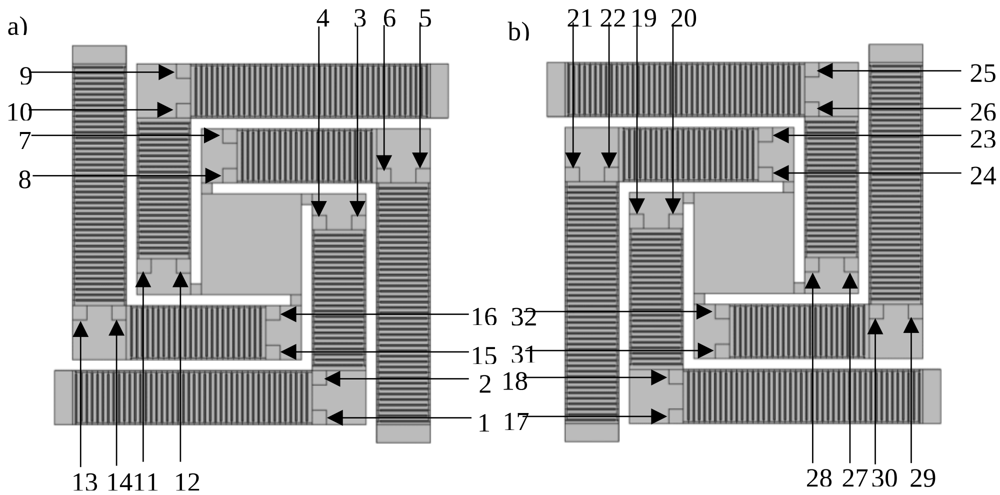

Figure 3.13 IDE pattern and number scheme on a) front and b) back surface of Piezo stage.

3.6.6 Meshing

Mesh convergence checked by doing free tetrahedral meshing of structure using different element size. We have used maximum element size as 1100 μm and minimum element size of 198 μm. The mesh convergence is checked using different set of element size and the results obtained from these cases shows the average difference of only 100 nm so here we have concluded that meshing is converged as the result difference is very small. Table 3.7 shows the mesh convergence results. Meshing shown in Figure 3.14 is free tetrahedral meshing with maximum element size as 1100 μm and minimum element size of 198 μm.

Table 3.7 Mesh Convergence Results.

SNo.	Maximum Element Size (μm)	Minimum Element Size (μm)	Element Growth rate	Curvature Factor	Resolution of Narrow Region	Results (μm)
1	1900	200	1.7	0.8	0.3	28.8
2	1100	198	1.5	0.6	0.5	29
3	880	110	1.45	0.5	0.6	29.1

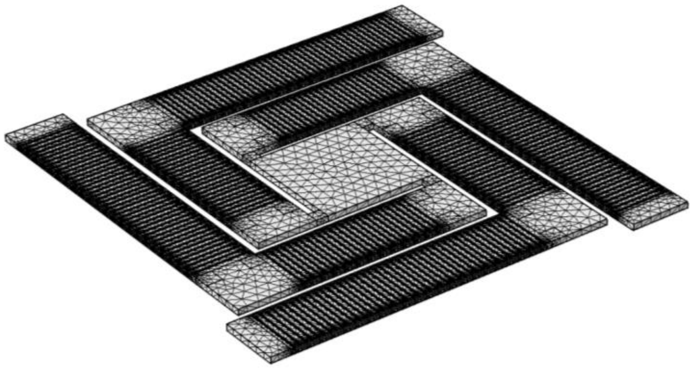

Figure 3.14 Meshing of Piezo Stage.

3.6.7 Boundary conditions

The analysis involves piezoelectric material which is electromechanical in nature. Different sets of mechanical and electrical boundary conditions have been used to produce different results which are explained in the Table 3.8. The mechanical boundary conditions are imposed by constraining all displacement of one side of the beam to define a fixed-point case while all other surfaces are free. For the electrical boundary condition, electric potentials are given to the top surface of the actuator where electrodes are made. The numbering of electrodes is shown in Figure 3.13 and the electrical constraints are shown in Table 3.8.

Table 3.8 Electrical Constraints.

SNo.	Actuation	Potential		
		+40V	-40V	Ground
1	X Tilt	1, 7, 11, 13, 19, 21, 25, 31	3, 5, 9, 15, 17, 23, 27, 29	2, 4, 6, 8, 10, 12, 14, 16, 18, 20, 22, 24, 26, 28, 30, 32
2	Y Tilt	1, 5, 11, 15, 19, 23, 25, 29	3, 7, 9, 13, 17, 21, 27, 31	
3	Z Translation	1, 5, 9, 13, 19, 23, 27, 31	3, 7, 11, 15, 17, 21, 25, 29	

3.6.8 Simulation Results for IDE based Piezo Stage

The static analysis shows that the piezo stage has been deflected in X, Y, Z directions. Figure 3.15 shows contour plots showing the surface displacement of the piezoelectric stage.

Simulation results in Table 3.9 shows that X Tilt, Y Tilt and Z translation are achieved by this structure with the magnitude of 38.9 (0.556º), 38.9 (0.556º) and 28.4 micrometres respectively for an actuation potential of 40 volts.

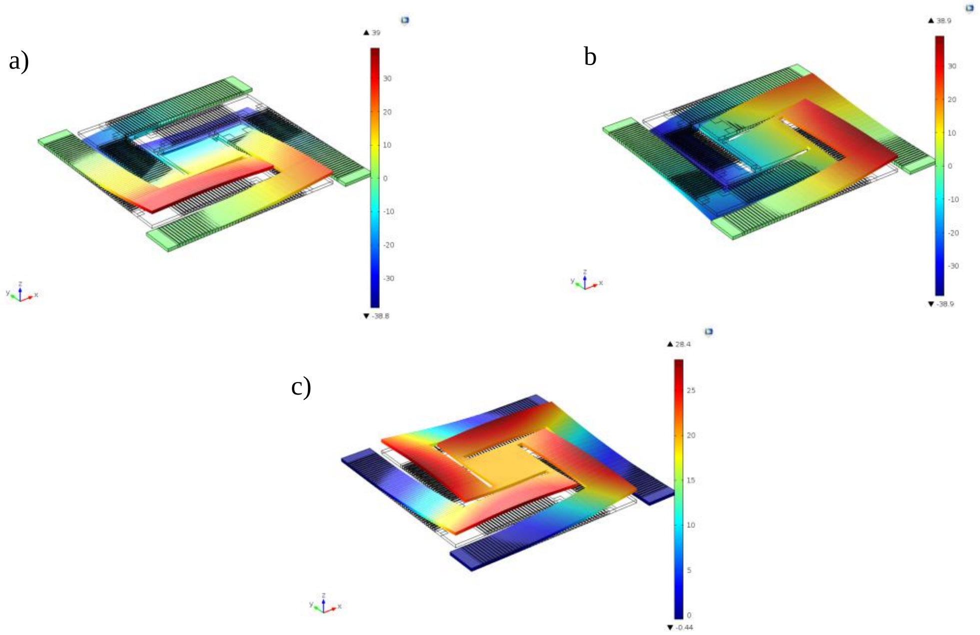

Figure 3.15 Contour plots showing the surface displacement of the piezoelectric stage when actuated at 40 volts DC: (a) X-tilt, (b) Y-tilt and (c) Z-translation.

Table 3.9 Simulation Results for IDE based Piezo Stage.

SNo,	Actuation	Result
1	X Tilt	38.9 µm (0.556º)
2	Y Tilt	38.9 µm (0.556º)
3	Z translation	28.4 µm

Chapter 4

Challenges in Fabrication of Piezo Stage

4.1. Introduction

In this chapter, challenges in the fabrication of piezoelectric stage is discussed. The various microfabrication techniques for the fabrication of Piezo stages have been discussed in Section 2.6. We have selected Abrasive Water Jet Machining (AWJM) for the fabrication of structure on the Piezo Plate. Following are the reasons that supports the selection of AWJM for fabrication:

i) Wet etching is not suitable because of the thickness of sample i.e. 191 μm. This will produce higher undercut ratio resulting in loss of material and symmetry of the device.

ii) Listed results in literature of DRIE using Cl_2 gas have better etching characteristics than with SF_6 gas. However, the side wall verticality, etching depth of over 100 μm is difficult to etch and lower etch rate are of main concern. We only have the facility with SF_6 as an etching gas.

iii) USM or Micro-powder blasting to fabricate the device are not available at our centre thus AWJM is used for making of the device.

Due to limited available resources for the fabrication of the device, AWJM is used for making piezo stage. We have to make some necessary changes in the design feature of the stage. The changes are made by considering the minimum cutting width available for AWJM (that is 1.5 mm). Figure 4.1 shows the modified design of the Piezo stage. For this the foot print of the device has been increased to 35x35 mm^2, and the width of L shaped actuators has been kept 2 mm. The simulation results of modified design are given in Appendix C.

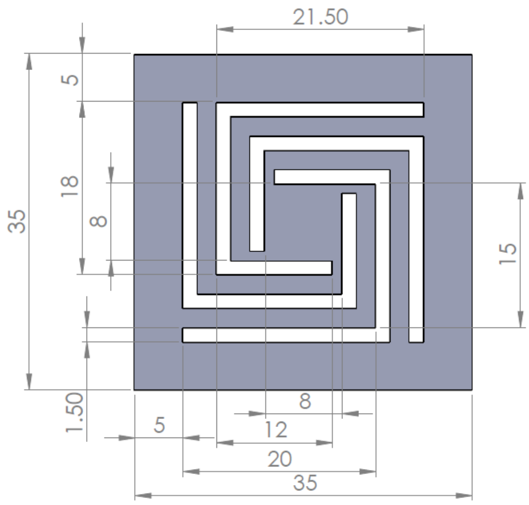

Figure 4.1 Modified dimensions of Piezo Stage.

4.2. Methodology for fabrication of piezoelectric stage

Fabrication of piezoelectric stage is done by producing device structure on monolithic plate of PZT-5H using AWJM process on which electrode pattern is to be made. Electrode pattern has to be made by using UV lithography. Gelatine mask has to be used for UV-lithography followed by etching of Nickle. Fabrication process of piezoelectric stage is shown in Figure 4.2. Step by step fabrication process is explained in details in following section of this chapter.

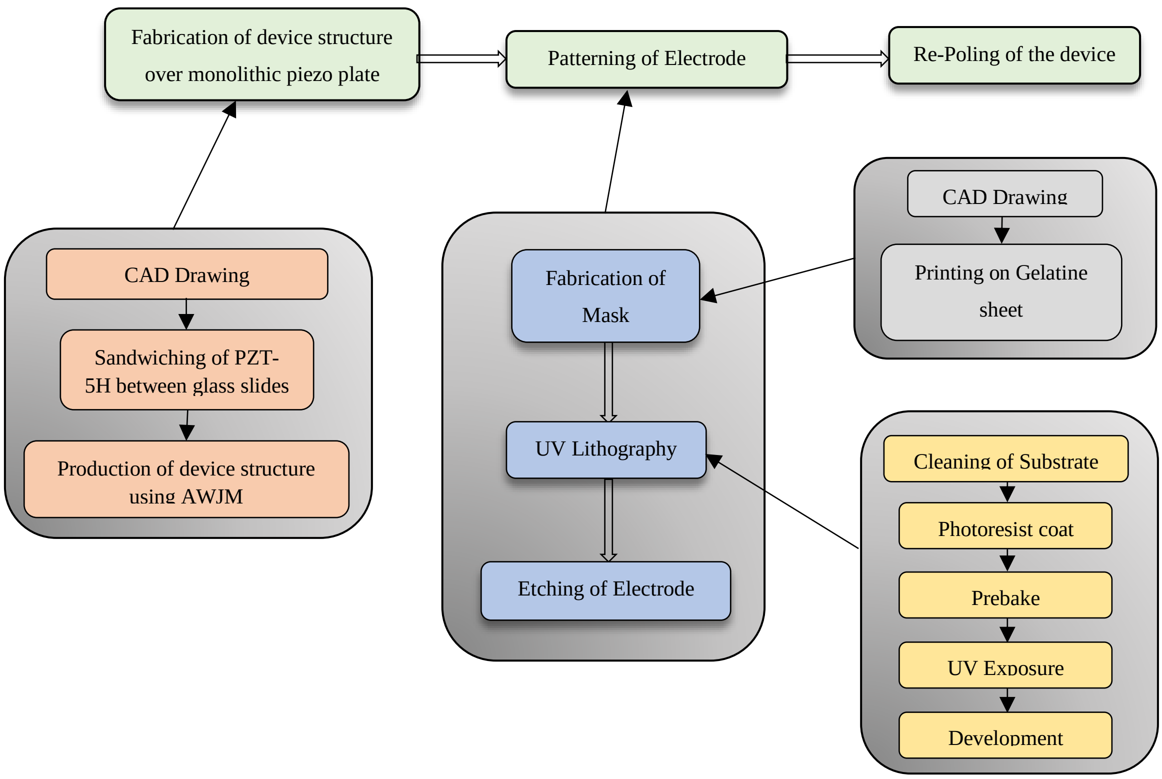

Figure 4.2 Block diagram showing the flow chart of fabrication steps for Piezo Stage.

4.2.1 AWJM of Piezo Plate

The device structure on which electrode has to be patterned is made from a monolithic plate of piezoelectric material PZT-5H (PiezoSystem Inc.). As the dimensions of the piezo plate is 76x76 mm^2 and thickness of the piezo plate is 191 µm, we have decided to sandwich the plate between two glass slides of dimension 80x80 mm^2 and having a thickness of 3 mm each to provide stability and strength against the shocks and impacts of AWJM. For the bonding purpose of piezo plate and glass slides we have used a chemical called CynoAcylate which is generally known as Feviquick 203. CynoAcrylate is used for the bonding purpose because it can be easily removed later by dissolving it in Acetone solution. Figure 4.3 shows the imported piezo plate PZT-5H and Figure 4.4 shows the sandwich structure of piezo plate between glasses.

a) b)

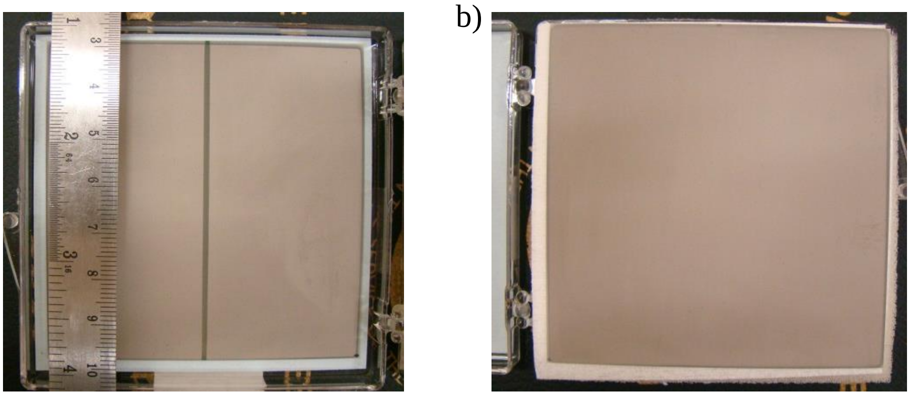

Figure 4.3 (a) Front and (b) back of PZT-5H plate.

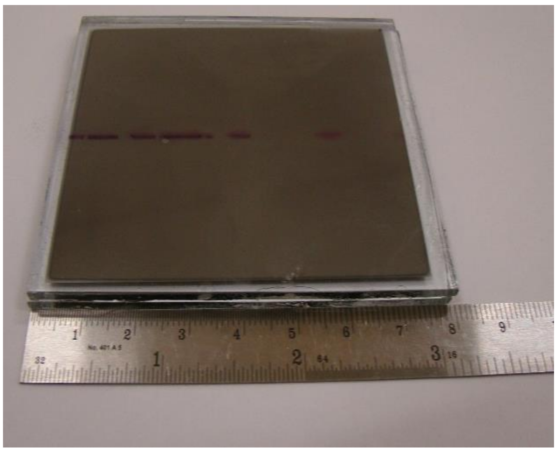

Figure 4.4 PZT-5H plate sandwiched with glass slides,

We have optimised the parameter of AWJM on different fixture materials like Aluminium, Acrylic and to obtain the desired structure of the device on the piezo plate in one run. The abrasive material used for cutting purpose is Garnets which is a naturally occurring chemical compound of silica found at sea shores and sea beds. The feed rate of abrasive is kept constant throughout the process and is 250 gm/min for piercing and cutting. Figure 4.5 shows the schematic of fixture mounting used for performing AWJM and.

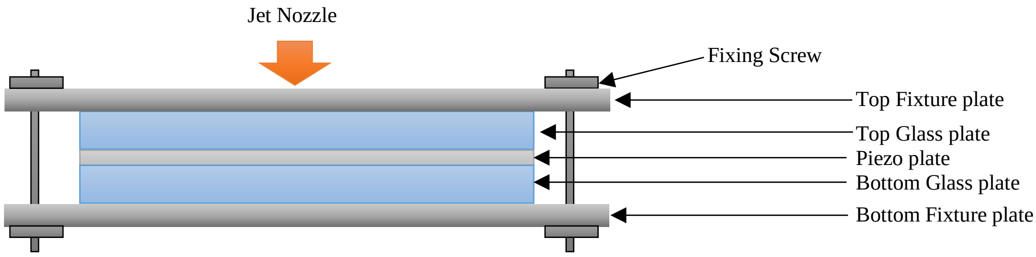

Figure 4.5 Schematic diagram of Fixture used for AWJM.

Initially a test run has been done using two bonded layers of glass without the PZT sample sandwiched in it to obtain the desired results. For first run, Aluminium plates of thickness 2 mm is used as fixture plates. The test sample of glass has been broken in that experiment because of chipping and burrs formation in aluminium plates near the cutting edges. Figure 4.6 shows the results of AWJM using aluminium as fixture and broken sample of glass.

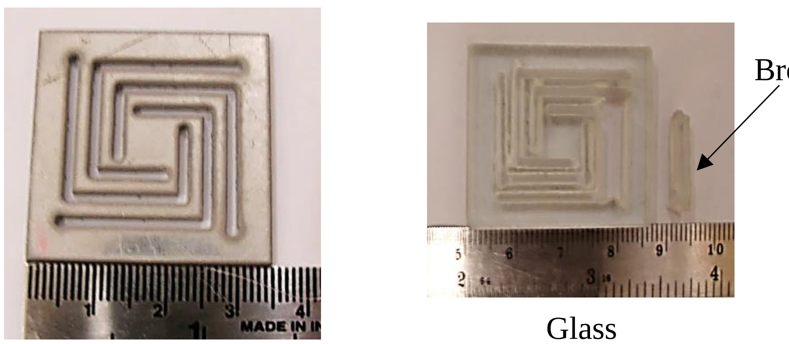

Figure 4.6 AWJM results for Aluminium as fixture plates.

To eliminate this issue, Acrylic is used as fixture plates. This allows us to get smooth edges along the cut in the test sample. Figure 4.7 shows the result of AWJM using acrylic as fixture plates. Various experiments have been done by changing the thickness of fixture plate and material to obtain desired structure on test sample (glass without PZT) and parameters are shown in Table 4.1.

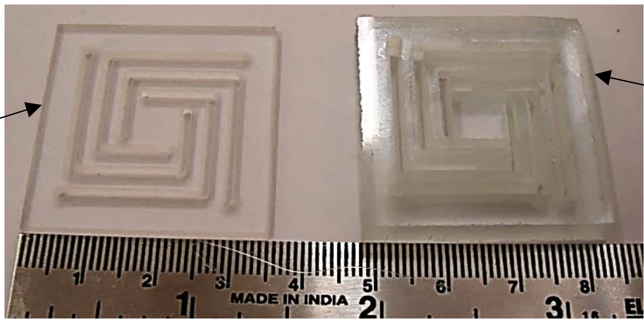

Figure 4.7 AWJM results for Acrylic as fixture plates.

Table 4.1 Parameters and results of AWJM.

SNo.	Material	Thickness (mm)	Pressure (bar)
1	Aluminum	2	1000
		4	1200
2	Acrylic	2	400-500
		4	700-800
3	Brass	0.3	600-700

With the help of these parameters obtain from different experiments, we cut the sample of PZT-5H with AWJM using a pressure of 800 bar. Figure 4.8 shows the device structure of PZT plate sandwiched in glass slides and fabricated with the help of AWJM.

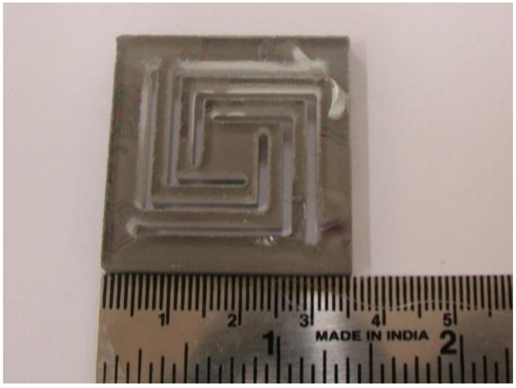

Figure 4.8 Device structure of PZT-5H.

We also try to fabricate device structure on Brass plate of thickness 300 μm to be used as a substrate for Unimorph stage. Figure 4.9 shows the fabricated device structure on Brass.

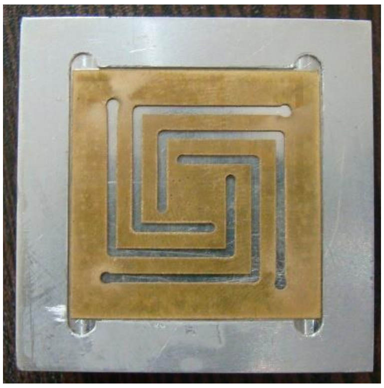

Figure 4.9 Device structure on Brass plate.

After the cutting of structure, we dipped the sample into Acetone solution for the separation of glass slides from the PZT structure. The sample was left in acetone for about 48 hours so the CynoAcrylate get dissolved in the solution resulting removal of bonded glass slides from PZT. Figure 4.10 shows the end results of the removal process.

When we separated the glass slides from PZT structure, it was found that the structure is broken into pieces. Because of the limited available raw material and facilities, we are unable to fabricate the device in the given course of time, so we tried an alternative method.

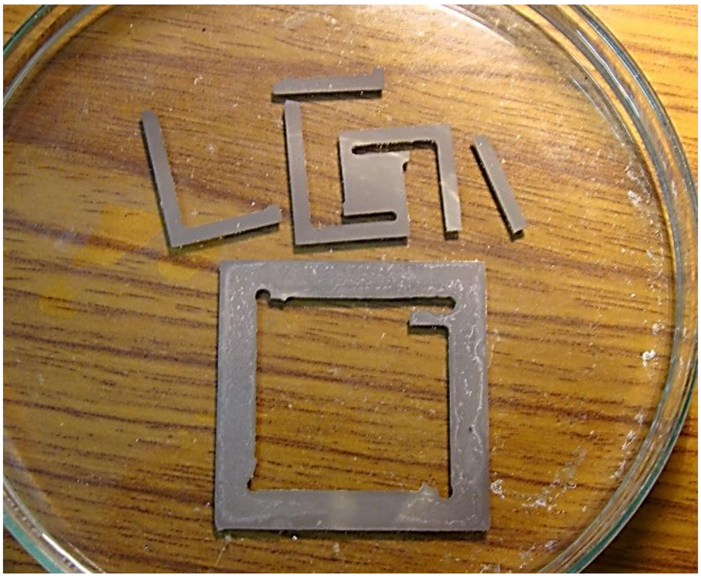

Figure 4.10 Results of separation of glass slides from PZT-5H.

4.3 Fabrication of Piezo Stage by alternative technique due to failure of AWJM

We fabricated simple cantilever of PZT-5H from the broken pieces of the device for characterisation purpose and to be used in unimorph piezo stage. The size of the cantilevers is 15mmX2mm and 13mmX2mm. The cantilever is fabricated by cutting the sample in desired dimension using diamond saw and

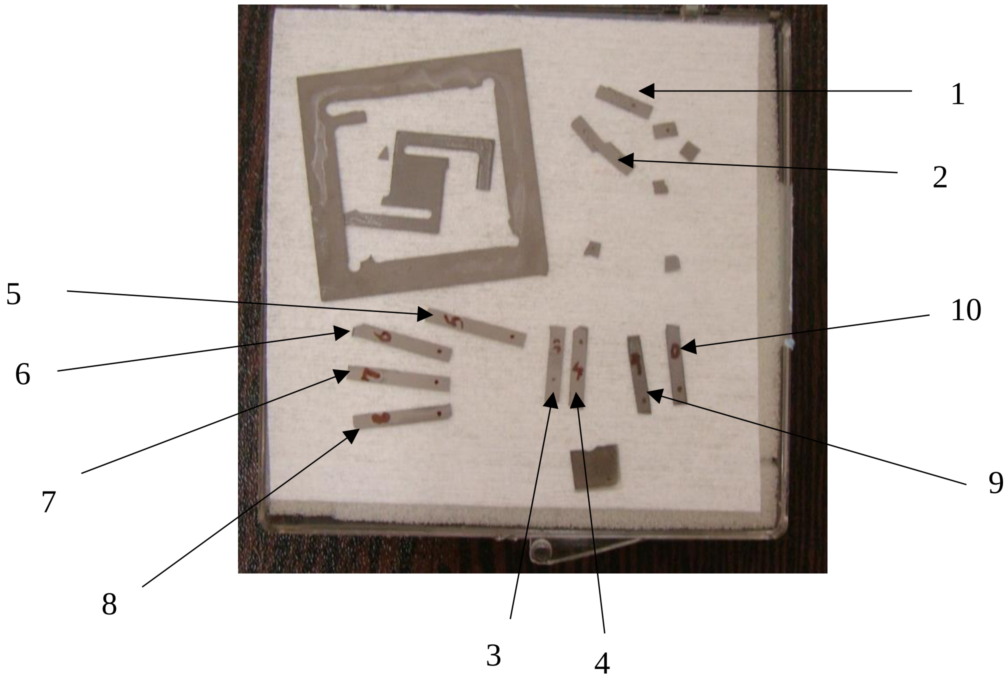

Figure 4.11 Cantilever legs fabricated from broken pieces of device structure.

then grinding to smoothen the edges. The Figure 4.11 shows the fabricated cantilever legs.

The d_{33} coefficient of these cantilever legs has been measured using BerlinCourt meter and the results are discussed in next section. Due to the damage during the grinding process some cantilever is broken down in between the characterisation as shown in Figure 4.9 (cantilever 1 and 2).

The various theories and results for the failure in fabrication of the device structure are discussed in details in next section.

4.4 Result and discussion

The results obtained from the simulation and fabrication steps and various challenges faced during the fabrication procedure is discussed in this section.

4.4.1 Simulation Results

Transverse bending for a monolithic layer of piezoelectric material has been obtained by using IDE patterns which is impossible by using PPE for a monolithic layer. The simulation results obtained in Table 3.3 shows that higher amount of actuation can be obtained for a monolithic layer of PZT using IDE on both surface of actuator than by morphing two layers of equal thickness and actuating by PPE. However, it is also observed that for actuator having equal thickness of monolithic and unimorph/bimorph design, the results are better for PPE case. Furthermore, the IDE geometry also plays a great role in actuation motion which was discussed in Table 3.3. By varying the geometrical parameter of IDE different results can be obtained for the same input conditions. Using IDE patterns Monolithic Piezoelectric Stage is conceptualised and simulated and the results obtained in Table 3.9 for MPS shows promising application of the device in near future.

4.4.2 Results of AWJM

The device has not survived during the fabrication procedure using AWJM and the following may be the causes for that:

i) Because of the high pressure of cutting during AWJM and shocks and impacts generated during the cutting procedure.

ii) Piercing (First cut at the starting point of cutting track) and overrunning cause the generation of stress concentration because of the reduced width of beam at the fixed end of L shape actuators and turning/corner point of the cutting track.

iii) Use of CynoAcrylate: During the removal of bonding agent, CynoAcylate forms sticky substances when dissolved in Acetone. When the glass slides separated, because of this substance an external force comes into picture, that may also be a cause of device breaking.

iv) Chipping and Burring formation: Due to use of abrasive media chipping and burring is observed near the cutting edge of the sample which may resulting in damage of the sample. Because of this burr formation we have switched the fixture material to Acrylic in place of Aluminum or Glass to obtain better results.

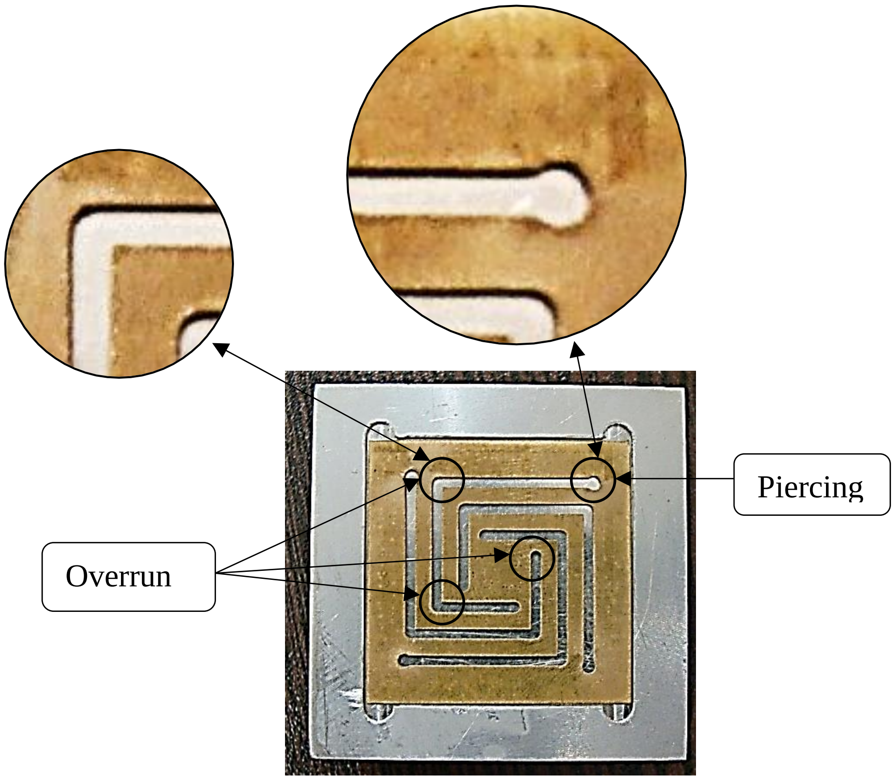

Figure 4.12 Piercing and Overrunning during AWJM.

The piercing and overrunning shown in Figure 4.10 cause loss of symmetry along with the stress concentration points which makes it further difficult to fabricate the device. This will also result in loss of accuracy and precision of the device performance.

4.4.3 Results of Alternative technique

The d_{33} coefficient of the fabricated cantilever has been measure using BerlinCourt meter and is found be in the range of 250-290 pC/m. The quoted coefficient of the material by the manufacturer is 640 pC/m. This de-poling of the material may happen because of the following reasons:

i) The various vibrational forces generated during the cutting procedure may cause the de-poling of the material.

ii) The material is sensitive to heat and use of dry grinding process for dimensioning may also results in loss of polarization.

iii) Use of dry powder grinding method: The liquid (oil) grinding method cannot be used to grind the sample for dimensioning purpose because the force generated during the grinding combined with the liquid media results in separation of glass bonded with the PZT sample. This cause the PZT to broke down into pieces. So, we used dry powder grinding method, which is effective for grinding the sample but generates greater amount of heat causing the sample to get depolarized.

This decrease in polarization results in decreased amount of actuation.

The Table 4.2 shows the results of d_{33} measurements of the 10 cantilever samples shown in Figure 4.9.

Table 4.2 Results of d33 measurement of cantilever legs.

Cantilever	D_{33} coefficient (pC/m)
1	261
2	268
3	227
4	265
5	253
6	286
7	286
8	286
9	276
10	290

Chapter 5

Conclusion and Future Work

5.1 Conclusion

In conclusion, a novel Monolithic Piezo Stage using L shape actuators has been conceptualized and simulated. The MPS is able to produce symmetric tilting of about 0.55 degrees along X and Y axis and translation of about 28 μm in Z direction when actuated at a potential of 40 volts in simulation for a given foot print of 20mmX20mm and thickness of 191 μm. With the use of IDE, the necessity to fabricate unimorph to produce out of plane motion has been eliminated which greatly enhance the performance of the device. The parameters of the IDE have a great influence on the performance of the device which has been studied and selected with great care with the help of various simulations. Although, in the current design we are only able to produce 3 DOF. However, there is great possibility lies in field of study and optimization to produce 6 DOF i.e. X and Y translation and Z rotation.

We have tried to fabricate the device using Abrasive Water Jet Machining but, we did not succeed because of various issues related with the fabrication procedure which was discussed. Alternative method to fabricate the device has also been tried using diamond saw cutting and grinding method which result in decrement of the piezoelectric coefficient.

The limited availability of resources, material and facilities limit us to fabricated, characterize and analyze the analytical data against experimental data for the device. However, in future there is strong possibility to fabricated the device and analyses the experimental data against analytical one.

5.2 Future Scope

The present L shaped Monolithic Piezoelectric Stage can be improved by the following:

- Precise fabrication technique is required to fabricate the device structure.
- Most of the parameters are limited to fabrication constrains. Use of advance micro-fabrication technology may further reduce the size of the stage.
- The performance of the device can be improved by further optimization and 6 DOF can be achieved.
- In addition, piezoelectric material with large d_{33} coefficient are preferred to further increase the performance.

References

[1] M. J. Madou, “Fundamentals of Microfabrication and Nanotechnology: Manufacturing Techniques for Microfabrication and Nanotechnology, vol. 2,” *Boca Raton, FL CRC Press. Llc*, 2011.

[2] W. J. Li and N. Xi, “Novel micro gripping, probing, and sensing devices for single-cell surgery.,” *Conf. Proc. IEEE Eng. Med. Biol. Soc.*, vol. 4, pp. 2591–2594, 2004.

[3] J. C. Chiou, C. C. Hung, C. Y. Lin, and Y. J. Lin, “Design, fabrication, and actuation of micro-electro-mechanical system-based image stabilizer,” *Jpn. J. Appl. Phys.*, vol. 49, no. 1 Part 1, 2010.

[4] T. C. Kenn and O. Yunfeng, “Suspension vibration compensation using a MEMS microactuator in hard disk drives,” pp. 757–762, 1999.

[5] C. K. Pang *et al.*, “Design, fabrication, sensor fusion, and control of a micro X-Y stage media platform for probe-based storage systems,” *Mechatronics*, vol. 19, no. 7, pp. 1158–1168, 2009.

[6] S. Tang *et al.*, “Design and implementation of fiber-based multiphoton endoscopy with microelectromechanical systems scanning,” *J. Biomed. Opt.*, vol. 14, no. 3, p. 34005, 2009.

[7] J. Tang, S. R. Green, and Y. B. Gianchandani, “Miniature wireless magnetoelastic resonant motor with frequency selectable bidirectional rotation,” *J. Microelectromechanical Syst.*, vol. 22, no. 3, pp. 730–738, 2013.

[8] S. Piratla, A. Lal, and M. Pandey, “Nanogap Ultrasonic Actuator for Non-Contact Control of Levitated Inertial Sensor Rotor,” *Hilt. Head*, no. January 2012, pp. 82–85, 2012.

[9] M. Bale and R. E. Palmer, “Deep plasma etching of piezoelectric PZT with SF[sub 6],” *J. Vac. Sci. Technol. B Microelectron. Nanom. Struct.*, vol. 19, no. 6, p. 2020, 2001.

[10] A. R. Bhatti, M. Mott, J. R. G. Evans, and M. J. Edirisinghe, "PZT pillars for 1-3 composites prepared by ink-jet printing," *J. Mater. Sci. Lett.*, vol. 20, no. 13, pp. 1245–1248, 2001.

[11] T. Li and Y. B. Gianchandani, "A die-scale micromachining process for bulk pzt and its applicatiun to in-plane actuators," *IEEE J. Microelectromechanical Syst.*, vol. 15, no. 3, pp. 605–612, 2006.

[12] D. W. Zeng, K. Li, K. C. Yung, H. L. W. Chan, C. L. Choy, and C. S. Xie, "UV laser micromachining of piezoelectric ceramic using a pulsed Nd : YAG laser," *Appl. Phys. a-Materials Sci. Process.*, vol. 78, no. 3, pp. 415–421, 2004.

[13] I. Misri, P. Hareesh, S. Yang, and D. L. DeVoe, "Microfabrication of bulk PZT transducers by dry film photolithography and micro powder blasting," *J. Micromechanics Microengineering*, vol. 22, no. 8, p. 85017, 2012.

[14] E. E. Aktakka, R. L. Peterson, and K. Najafi, "A 3-DOF piezoelectric micro vibratory stage based on bulk-PZT/silicon crab-leg suspensions," *Proc. IEEE Int. Conf. Micro Electro Mech. Syst.*, no. Figure 6, pp. 576–579, 2013.

[15] P. Hareesh, I. Misri, S. Yang, and D. L. Devoe, "Transverse interdigitated electrode actuation of homogeneous bulk PZT," *J. Microelectromechanical Syst.*, vol. 21, no. 6, pp. 1513–1518, 2012.

[16] N. Chidambaram, A. Mazzalai, D. Balma, and P. Muralt, "Comparison of lead Zirconate Titanate thin films for microelectromechanical energy harvester with interdigitated and parallel plate electrodes," *IEEE Trans. Ultrason. Ferroelectr. Freq. Control*, vol. 60, no. 8, pp. 1564–1571, 2013.

[17] A. Kholkin, AL and Pertsev, NA and Goltsev, "Piezoelectricity and Crystal Symmetry," in *Piezoelectric and Acoustic materials for transducer application*, Springer US, 2008, pp. 17–38.

[18] A. J. Moheimani, S.O. Reza, Fleming, *Piezoelectric Transducers for*

Vibration Control and Damping. Springer US, 2006.

[19] J. G. Smits, S. I. Dalke, and T. K. Cooney, “The constituent equations of piezoelectric bimorphs,” *Sensors Actuators A. Phys.*, vol. 28, no. 1, pp. 41–61, 1991.

[20] L. Mengwei *et al.*, “Piezoelectric microcantilevers with Two PZT thin-film elements for microsensors and microactuators,” in *Proceedings of 1st IEEE International Conference on Nano Micro Engineered and Molecular Systems, 1st IEEE-NEMS*, 2006, pp. 775–778.

[21] B. S. Lee, S. C. Lin, and W. J. Wu, “Fabrication and evaluation of a MEMS piezoelectric bimorph generator for vibration energy harvesting,” *J. Mech.*, vol. 26, no. 4, pp. 493–499, 2010.

[22] J. F. Tressler, S. Alkoy, and R. E. Newnham, “Piezoelectric sensors and sensor materials,” *J. Electroceramics*, vol. 2, no. 4, pp. 257–272, 1998.

[23] Y. Yee, H. J. Nam, S. H. Lee, J. U. Bu, and J. W. Lee, “PZT actuated micromirror for fine-tracking mechanism of high-density optical data storage,” *Sensors Actuators, A Phys.*, vol. 89, no. 1–2, pp. 166–173, 2001.

[24] T. Naono, T. Fujii, M. Esashi, and S. Tanaka, “Non-resonant 2-D piezoelectric MEMS optical scanner actuated by Nb doped PZT thin film,” *Sensors Actuators, A Phys.*, vol. 233, pp. 147–157, 2015.

[25] A. Arevalo and I. G. Foulds, “Parametric Study of Polyimide – Lead Zirconate Titanate Thin Film Cantilivers for Transducer Applications,” pp. 1–5, 2013.

[26] A. Mazzalai, N. Chidambaram, and P. Muralt, “Conception of an interdigitated electrodes based cantilever for piezoelectric energy harvesting,” *Proc. power MEMS*, pp. 1–4, 2011.

[27] W. Beckert and W. S. Kreher, “Modelling piezoelectric modules with interdigitated electrode structures,” *Comput. Mater. Sci.*, vol. 26, no. SUPPL., pp. 36–45, 2003.

[28] E. E. Aktakka, R. L. Peterson, and K. Najafi, “Wafer-level integration of

high-quality bulk piezoelectric ceramics on silicon," *IEEE Trans. Electron Devices*, vol. 60, no. 6, pp. 2022–2030, 2013.

[29] J. Zhang, W. Ren, X. Jing, P. Shi, and X. Wu, "Deep reactive ion etching of PZT ceramics and PMN-PT single crystals for high frequency ultrasound transducers," *Ceram. Int.*, vol. 41, pp. S656–S661, 2015.

[30] S. Wang, "Deep Reactive Ion Etching of Lead Zirconate Titanate Using Sulfur Hexafluoride Gas," vol. 41, pp. 1339–1341, 1999.

[31] E. E. Aktakka, R. L. Peterson, and K. Najafi, "A 6-Dof Piezoelectric Micro Vibratory Stage Based On Multi-Axis Distributed-Electrode Excitation Of Pzt / Si Unimorph T-Beams," no. June, pp. 1583–1586, 2013.

Appendix A

The utilisation of d_{31} piezoelectric coefficient for PPE and d_{33} coefficient for IDE to produce deformation in actuator.

i) PPE over a monolithic layer of Piezoelectric actuator.

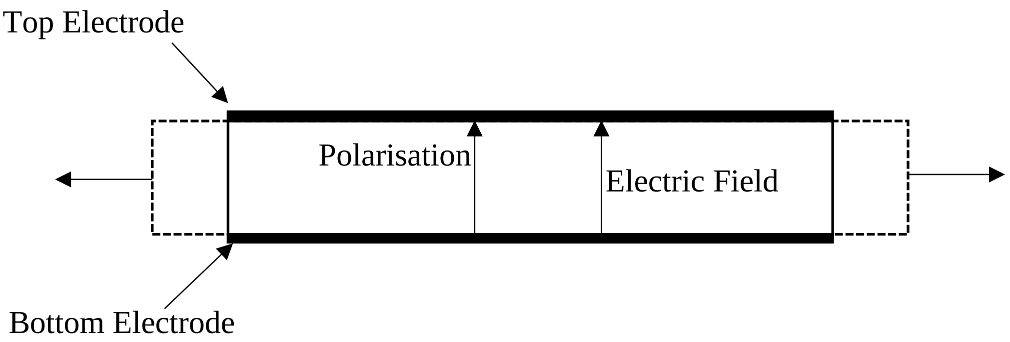

ii) IDE over single surface of a monolithic layer of Piezoelectric actuator.

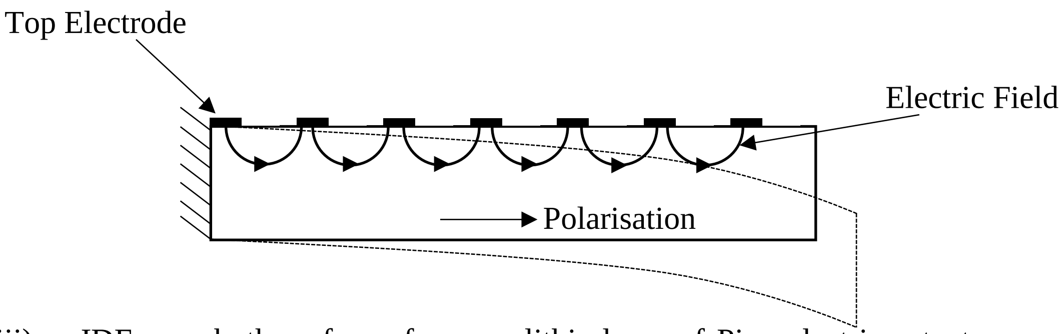

iii) IDE over both surface of a monolithic layer of Piezoelectric actuator having same polarity.

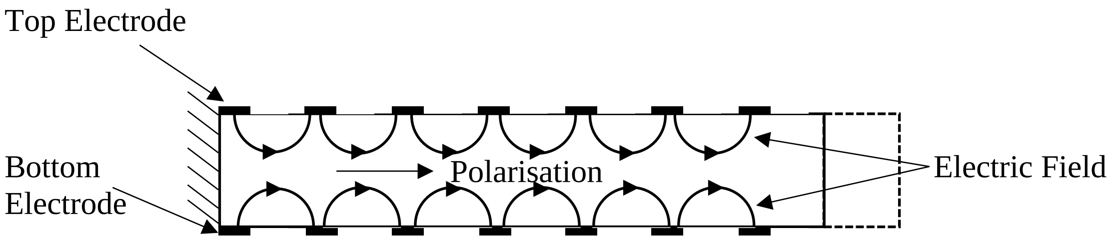

iv) IDE over both surface of a monolithic layer of Piezoelectric actuator having opposite polarity.

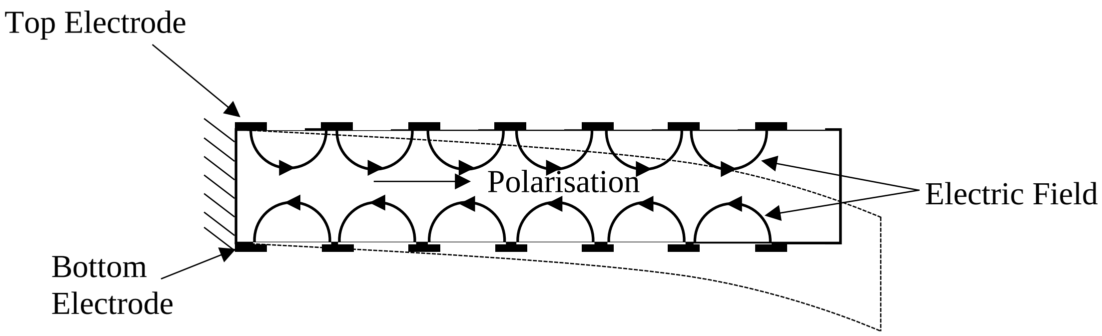

Appendix B

Electric field line plots for different actuation methods.

i) Contour plots for PPE actuator.

Unimorph

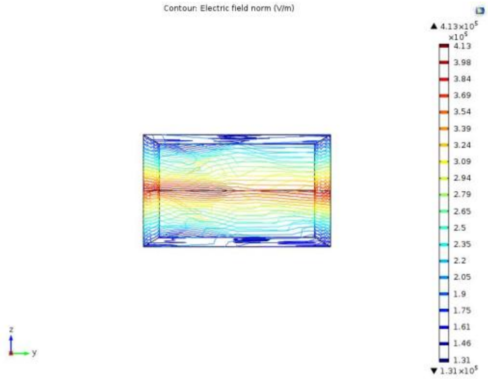

Bimorph

ii) Contour plots for IDE actuators.

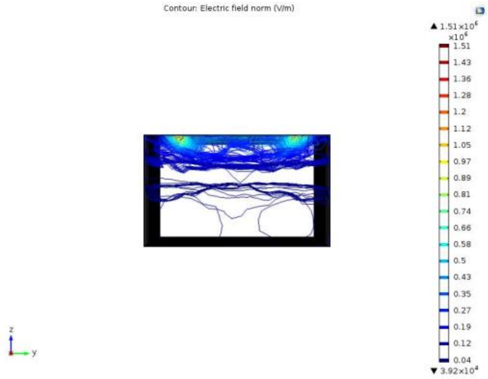

Unimorph

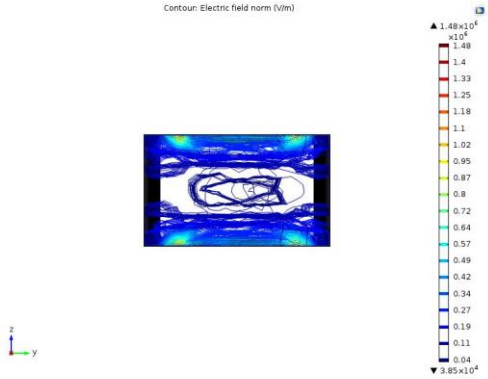

Bimorph

iii) Isosurface plots for IDE actuators.

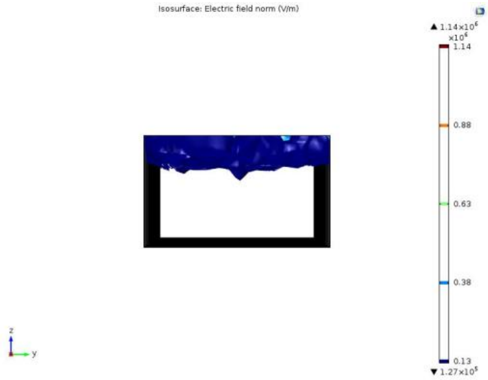

Unimorph

Bimorph

Appendix C

Simulation results of piezo stage having foot print of 35 mm^2. Having IDE patterns on one surface only and actuated at a potential of 40 volts.

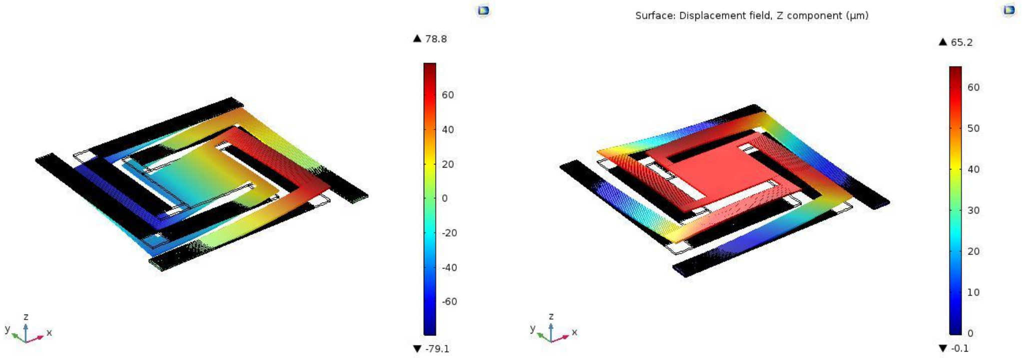

SNo,	Actuation	Result
1	Tilt	0.515º
2	Translation	65.2 µm

Appendix D

Mask images for IDE patterns for MPS.

1. For stage of foot print 10mmX10mm.

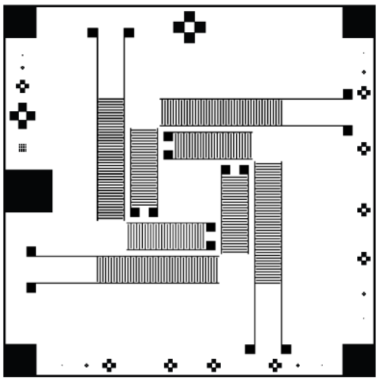

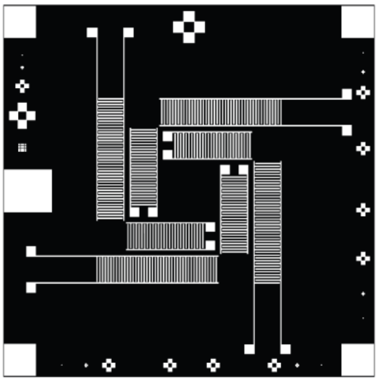

2. For stage of foot print 35mmX35mm.